Strong long-lived Kuroshio-shed anticyclonic eddies and their re-intensification in the northern South China Sea

Xiangpeng Wang[1, 2], Yan Du[1, 3*], Xiaoming Zhai[2], Yuhong Zhang[1, 3], Minyang Wang[1]

1. Guangdong Provincial Key Laboratory of Remote Sensing and Big Data, State Key Laboratory of Tropical Oceanography, South China Sea Institute of Oceanology, Chinese Academy of Sciences, Guangzhou, China.

2. School of Environmental Sciences, Centre for Ocean and Atmospheric Sciences, University of East Anglia, Norwich, United Kingdom.

3. College of Marine Science, University of Chinese Academy of Sciences, Beijing, China.

*Corresponding author: Yan Du (duyan@scsio.ac.cn)

Abstract: The Kuroshio anticyclonic eddy shedding event occurs nearly every winter in the northeastern South China Sea (SCS). Between 1993 and 2023, 27 prominent Kuroshio-shed anticyclonic eddies were identified based on satellite altimetry data. These eddies propagated southwestward along the continental slope and typically dissipated near the Xisha Islands in spring, with an average lifespan of approximately 89 days. Notably, three exceptionally strong and long-lived eddies were observed in 2010, 2017, and 2021, each persisting for more than 180 days. Unlike the regular eddies that dissipated upon encountering the Xisha Islands, these long-lived eddies slightly moved eastward along the topography and re-intensified during summer. Eddy-current interactions and eddy mergers were identified as the primary mechanisms driving their re-intensification. Hydrographic observations revealed that the long-lived Kuroshio eddies evolved seasonally from surface-intensified to subsurface-intensified eddies, ultimately exhibiting a lens-shaped structure in the upper 300 m. The intense lens core was enclosed by a strong potential vorticity (PV) gradient, acting as a PV barrier that prevents water exchange between the eddy interior and its surroundings. Despite undergoing interactions that re-intensified the eddy, the eddy core maintained its high-salinity and low-PV characteristics. Such intrinsic eddies may play an important role in local air-sea interactions, heat-salt balances, and biogeochemical processes.

Significance Statement

The Kuroshio intrusion and its associated anticyclonic eddy shedding are key dynamic processes in the northern South China Sea (SCS). This study examines the statistical characteristics of Kuroshio-shed anticyclonic eddies, focusing on the evolution of those that are strong and long-lived. Most Kuroshio eddies form in winter and dissipate by spring, but some strong eddies re-intensify east of Xisha Islands during summer, allowing persistence into autumn. Eddy-current and eddy-eddy interactions are primary mechanisms driving their re-intensification. The re-intensified eddies retain Kuroshio water characteristics within their cores due to the potential vorticity (PV) barrier, while the merging water wraps around the eddy periphery. This study highlights the evolution of Kuroshio eddies in the SCS and their interactions with the surrounding environment.

1. Introduction

Mesoscale eddies are a crucial component of the ocean circulation system, typically characterized by spatial scales ranging from tens to hundreds of kilometers and temporal scales from days to months (Chelton et al., 2007, 2011; Robinson, 1983). They play a vital role in ocean dynamics and exert a profound impact on marine ecosystems by redistributing nutrients, heat, salt, and other oceanic properties (Dong et al., 2014; Gaube et al., 2013; McGillicuddy, 2016; Zhang et al., 2014).

The South China Sea (SCS) is the largest marginal sea in the northwestern Pacific Ocean. Both observational and modeling studies reveal that the SCS is abundant with eddy activities (Chu and Fan, 2001; Hu et al., 2011; Lin et al., 2015; Wang et al., 2003). Based on satellite altimetry data, Chen et al. (2011) found that mesoscale eddies are mainly generated in the northeastern and southwestern regions of the SCS. Correspondingly, the region southwest of Taiwan Island was observed to have strong eddy kinetic energy (Chen et al., 2009; Cheng and Qi, 2010). Nan et al. (2011b) analyzed the characteristics of mesoscale eddies southwest of Taiwan Island. They pointed out that anticyclonic eddies occurred more often in winter, while cyclonic eddies were more frequent in summer. Compared with the direct local wind forcing, the Kuroshio intrusion appears to be a dominant factor for eddy formation in this area.

Originating from the North Equatorial Current, the Kuroshio carrying the northwestern Pacific water intrudes into the SCS through the Luzon Strait (Centurioni et al., 2004; Nan et al., 2015; Qu et al., 2000; Xue et al., 2004). Based on multiple satellite observations, previous studies pointed out that the Kuroshio intrusion in the Luzon Strait generally presents different

spatial patterns, like leaking, leaping, and looping paths (Caruso et al., 2006; Nan et al., 2011a). Of the three patterns, the Kuroshio looping path is primarily witnessed in the northeastern SCS during winter and is often accompanied by anticyclonic eddy shedding (Jia and Chassignet, 2011; Yuan et al., 2006; Zhang et al., 2013).

The Kuroshio-shed anticyclonic eddies can transport large amounts of warm, salty, and oligotrophic Kuroshio water to the interior SCS, significantly affecting the hydrodynamic and biogeochemical processes of the region (Wang et al., 2021; Xiu and Chai, 2011; Zhang et al., 2013, 2017). Therefore, these eddies have received substantial attentions. Li and Wu (1989) first introduced the Kuroshio loop current (KLC) to describe the anticyclonic circulation pattern enclosed by inflow and outflow currents through the Luzon Strait. They suggested the possibility of eddy shedding from the KLC. Through analyzing the hydrographic data, Li et al. (1998) inferred that an anticyclonic eddy was shed from the Kuroshio, with its influence depth reaching 1000 m in the northeastern SCS. However, a later study by Yuan et al. (2007), which tracked eddies using altimeter data, revealed that the eddy observed by Li et al. (1998) was not shed from the KLC but was the Luzon warm eddy. Jia and Liu (2004) found that the Kuroshio bend varied with time, and the anticyclonic eddies were periodically shed from the Kuroshio through satellite altimeter data. Using a nonlinear 2 and 1/2 layer model, they further examined the relationship between the Kuroshio transport and the eddy-shedding events, finding that frontal instability induced by the Kuroshio transport affects the separation of anticyclonic eddies (Jia et al., 2005). With the increase in field observations, more Kuroshio-shed anticyclonic eddies have been observed and reported in the SCS (e.g., Qiu et al., 2019; Wang et al., 2008; Zhang et al., 2016).

Through the synergetic analyses of mooring arrays, satellite data, and HYCOM products, Zhang et al. (2017) investigated the characteristics and mechanisms of KLC eddy shedding. They found that the generation and growth of the cyclonic eddy southwest of Taiwan facilitated the detachment of the anticyclonic eddy from KLC. Their study further suggested that the Kuroshio-shed anticyclonic eddy can result in a 0.24–0.38 Sv westward volume transport through the Luzon Strait, accounting for 6.8%–10.8% of the total transport in the upper layer. Recently, a strong KLC event occurred during the winter of 2020/21, accompanied by a lens-shaped cold-core anticyclonic eddy shedding into the SCS (Qi et al., 2022; Sun et al., 2021). Based on cruise observations and reanalysis data, Wang et al. (2023) found that the Kuroshio-shed anticyclonic eddies generated in winter evolve into subsurface-intensified eddies by late spring due to seasonal variations in sea surface heat flux and geostrophic adjustment.

Although a recent study by Tang et al. (2024) showed that submesoscale processes at the periphery of KLC can also transport significant amounts of heat and salt into the northeastern SCS, mesoscale eddies remain the primary carrier for long-distance transport of Kuroshio water into the SCS. Despite numerous studies on Kuroshio intrusion and its associated anticyclonic eddy shedding, most have concentrated on the eddy shedding stage. Our knowledge of the complete evolution of Kuroshio-shed anticyclonic eddies in the SCS, especially the strong long-lived ones, remains limited.

This study investigates the statistical characteristics of Kuroshio-shed anticyclonic eddies in the SCS and focuses on the evolution and re-intensification of strong long-lived cases. The rest of this paper is organized as follows. Section 2 introduces the data and methods. Section 3 presents the statistical results and the evolution of three long-lived eddies in the SCS. Finally, the discussion and conclusion are provided in Sections 4 and 5, respectively.

2. Data and Methods

a. Satellite altimetry data

Sea level anomaly (SLA) and surface geostrophic currents derived from satellite altimetry are widely used to detect mesoscale eddies (Chelton et al., 2011; Chen et al., 2011; Sun et al., 2017). This study used satellite altimeter data distributed by the Copernicus Marine Environment and Monitoring Service (CMEMS) to identify and examine the surface characteristics of Kuroshio anticyclonic eddies. The data product has merged different altimeter missions, including Jason, TOPEX/Poseidon, GFO, ERS, etc. This data spans from January 1993 to June 2023, with daily and 1/4° resolutions. SLA in this dataset is referenced to a 20-year mean (1993-2012).

b. In situ data

Argo is a global array of more than 3000 free-drifting profiling floats that measure the temperature and salinity on the upper 2000 m. Between July 2020 to April 2022, an Argo float (WMO number: 2902711) operated in the northeastern SCS, collecting 133 profiles at 5-day intervals. This float captured a prominent Kuroshio eddy shedding event in early 2021 (Fig. 1a). For this study, the profiles, with a maximum depth of approximately 2,000 m, were linearly interpolated at 10 m intervals. The Argo data was sourced from the Coriolis Argo Global Data Assembly Centre (GDAC). The Argo profiles passed a series of quality controls, and only those flagged as good (quality flag = 1) were used for the present study.

Three targeted cruise surveys for a specific Kuroshio-shed anticyclonic eddy were conducted in the northern SCS on May 21-28, August 10-15, and September 9-14, 2021 (Fig. 1b-d), corresponding to different stages of the Kuroshio eddy. The first cruise corresponded to the stage when the eddy approached the Xisha Islands. The second and the third cruises were carried out after the eddy re-intensification. A total of six hydrographic transects (A, B, C, D, E, F) were obtained during three cruise surveys. The second cruise did not completely pass through the target anticyclonic eddy, but only the left half of the eddy was observed. Temperature and salinity profiles in the upper 2000 m were measured by the SeaBird 911 Plus conductivity–temperature–depth (CTD) instrument, with an effective vertical resolution of 1 m. Current velocities were measured using shipboard acoustic Doppler current profilers (SADCPs), which provided velocity data for the water column as follows: approximately 16–600 m (75 kHz, 8 m bin size) during the first cruise, 30–800 m (38 kHz, 16 m bin size) during the second cruise, and 14–200 m (150 kHz, 8 m bin size) during the third cruise.

The climatological temperature and salinity data from *World Ocean Atlas 2018 (WOA18)* were used to delineate the characteristics of the Kuroshio water and the SCS water. This data was acquired from the NOAA National Centers for Environmental Information (NCEI).

c. Reanalysis data

A 1/12° ocean reanalysis dataset from the CMEMS was used to investigate the dynamic mechanisms of eddy re-intensification in the SCS (Lellouche et al., 2021). The GLORYS12V1 product (GLOBAL_REANALYSIS_PHY_001_030) is based on the current real-time global forecasting CMEMS system. It has assimilated altimeter data (SLA), satellite SST, sea ice concentration, and vertical in situ temperature and salinity profiles. The GLORYS12V1 datasets include two versions: the first version provides daily data spanning from January 1993 to June 2021, while the second version is updated daily from July 2021 to October 2024. Notably, the evolution of the Kuroshio eddy in 2021 spanned both datasets (October 2020 - November 2021). However, the latter dataset inadequately captured the re-intensification process of the Kuroshio-shed eddy during the summer of 2021 (not shown). Consequently, we utilized a high-resolution analysis and forecasting dataset (GLOBAL_ANALYSIS_FORECAST_PHY_001_024), covering the period from 2019 to the present and also assimilating observational data, to analyze the re-intensification process of the shedding eddy in 2021. These datasets are in good agreement with the observations and have been widely used for the study of oceanic mesoscale eddies (e.g., Qiao et al., 2023; Potter et al., 2021; Wang et al., 2021 & 2023). The variables used in this study include daily sea surface

height (SSH), three-dimensional velocity, temperature, and salinity.

d. Identification of the Kuroshio anticyclonic eddies

To investigate the statistical characteristics of the Kuroshio anticyclonic eddies, we first identified all prominent Kuroshio eddy-shedding events based on 31-year historical altimeter data. The basic principle of eddy detection is to find appropriate closed SLA contours with a single core. Under the geostrophic assumption, the eddy streamlines correspond to the closed SLA contours. The eddy center is typically defined as the location of the local extremum in the SLA field (i.e., minimum for cyclonic eddies, maximum for anticyclonic eddies), or alternatively, as the extremum in the streamfunction field (maximum for cyclonic eddies, minimum for anticyclonic eddies) in subsurface layer. The eddy edge is defined as the outermost closed SLA (streamline) contour enclosing the eddy (Chelton et al., 2011; Ni et al., 2021). The SLA difference between the eddy center and the edge is defined as the eddy amplitude. With one day as a step, the centers of the same eddy are closest at two adjacent moments. When the amplitude is less than 2 cm, it is regarded as the demise time of the eddy. Based on this criterion, the eddy's trajectory can be tracked. More details about eddy identification and eddy-tracking procedure can be found in Chen et al. (2011). Here, only the anticyclonic eddies that are directly detached from the KLC are referred to as Kuroshio-shed anticyclonic eddies and are included in the statistics. The eddy shedding time is defined as the time when the eddy's SLA contours are completely separated from the Kuroshio. The lifetime of the eddy is defined as the duration between the shedding time and demise time. Eddies with a lifetime of no more than two weeks were excluded from our analysis. All the selected eddies have been subjected to a second-round manual inspection with the snapshots of SLA and sea surface currents to ensure that these eddies meet the criteria defined in this study.

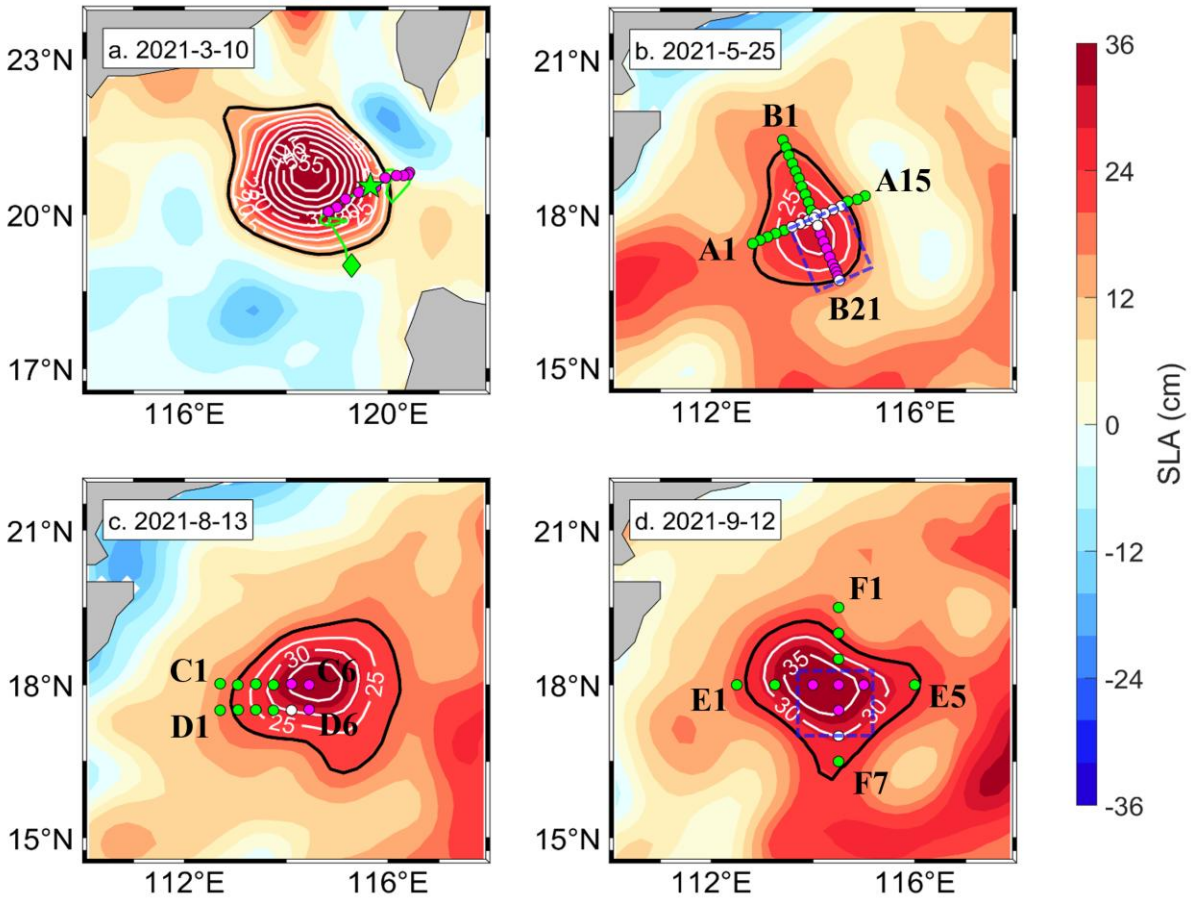

FIG. 1. Four stages of hydrographic observations. Color shading shows the SLA on a particular day during the observation period. White contours represent the closed SLA with 5-cm intervals associated with the eddy center. Black contour represents the eddy edge. (a) Argo observation. The green line is the trajectory of Argo float 2902711 from November 3, 2020, to June 12, 2021. The star and diamond denote the starting and ending positions, respectively. Pink dots denote the location of Argo float inside the eddy from February 1, 2021, to March 19, 2021. (b)-(d) Cruise observations during 21-28 May 2021, 10-15 August 2021, and 9-14 September 2021, respectively. Dots represent the CTD stations, whereas the pink, white, and green dots represent stations at the core, edge, and outside of the lens-shaped structure, respectively. The dashed blue box in panels (b) and (d) highlights the region of lens-shaped core.

e. Calculation of dynamic parameters

The relative vorticity (ζ), Rossby number (R_O) and potential vorticity (PV) are crucial for understanding dynamic characteristics. In three-dimensional gridded data, the calculation of relative vorticity can be calculated as follows:

$$\zeta = \frac{\partial v}{\partial x} - \frac{\partial u}{\partial y}, \qquad (1)$$

Where u, v are zonal and meridional components of current. Subsequently, the Rossby number and PV can be calculated as:

$$R_O = \frac{\zeta}{f}, \quad (2)$$

$$PV = -\frac{f+\zeta}{\rho}\frac{\partial \rho}{\partial z}, \quad (3)$$

where f is the Coriolis parameter, and ρ is the potential density.

For the calculation of relative vorticity in observational sections, we follow the methodology outlined by Nencioli et al. (2008), where the relative vorticity is estimated in cylindrical coordinates as follows:

$$\zeta = \frac{v_n}{r} + \frac{\partial v_n}{\partial r}, \quad (4)$$

where v_n is the orbital velocity observed by SADCP, and r is the radial distance referenced to the eddy center. Note that the eddy center is defined here as the location where the orbital velocity approaches zero, as the observational sections in this study generally pass through it.

3. Results

a. Characteristics of Kuroshio Anticyclonic Eddies in the SCS

Based on historical satellite altimeter observations, 27 prominent Kuroshio-shed anticyclonic eddies were screened out between 1993 and 2023. The comprehensive details, including the eddy's generation, shedding and demise dates, lifespan, shedding amplitude, and demise location, are documented in Table 1 of the Supplemental Material. The results are generally consistent with those reported by Zhang et al. (2017), who identified 19 prominent KLC eddy shedding events between 1992 and 2014 based on altimeter SSH and SLA. We further quantified the typical scales of these eddies at their shedding time, which corresponds to their mature stage. The Kuroshio-shed eddies exhibit radii ranging from 59 to 160 km, with an average radius of 106 km. The maximum geostrophic velocities range between 0.36 and 1.14 m/s, with a mean of 0.76 m/s. The minimum Rossby number in some cases is less than –0.5, reaching down to –0.6, indicating that inertial forces are significant and comparable to the geostrophic balance in the Kuroshio eddy dynamics under certain conditions.

Figure 2 illustrates the evolution of each Kuroshio-shed eddy over its lifespan. These eddies typically originate within the KLC during autumn and winter, reaching their peak intensity at the shedding stage. After detaching from the KLC, they decay rapidly and generally dissipate by the following spring or summer. Only three instances occurred during the summer, with two in August 2004 and one in August 2016. On average, the eddy shedding events occur nearly once a year. However, in 2004, 2015, and 2016, two or more instances of anticyclonic

eddy shedding were observed. Between 1993 and 2000, the Kuroshio eddy shedding events occurred almost once every two years, with a relatively strong eddy intensity. From 2001 to 2009, the frequency of shedding events was low, and the eddy intensity was weak. After 2010, both the frequency and the intensity of shedding events increased. The interannual and decadal variabilities in Kuroshio eddy shedding events may be related to the strength of Kuroshio intrusion induced by large-scale climate variability in the Pacific Ocean, such as El Niño–Southern Oscillation (ENSO) and Pacific Decadal Oscillation (PDO) (Nan et al., 2013; Qu et al., 2004; Wu, 2013).

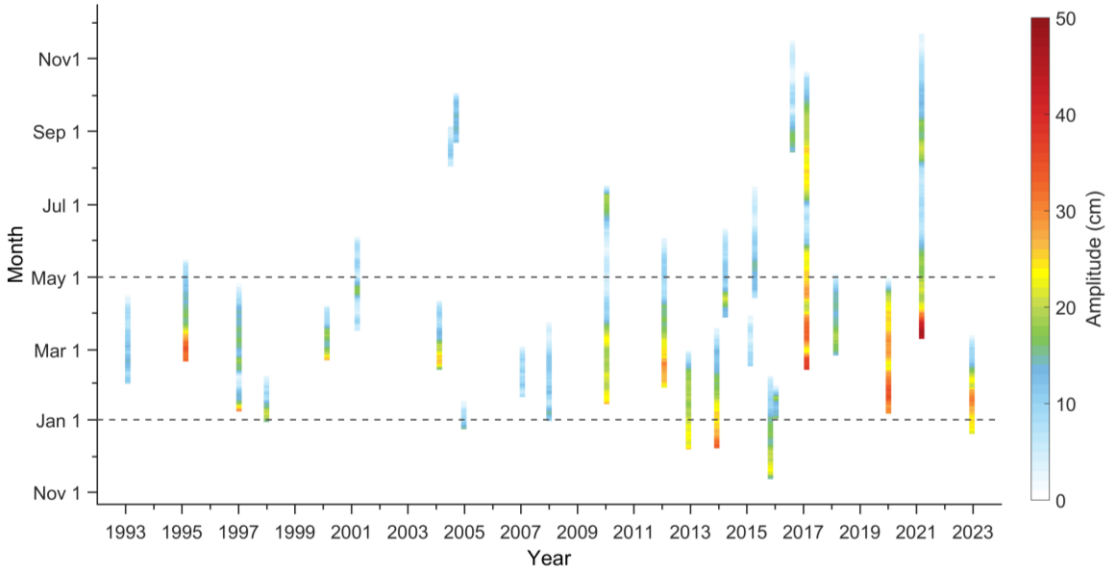

FIG. 2. Information of the prominent Kuroshio-shed anticyclonic eddies during 1993-2023. The color of the bar represents the time-dependent amplitude of the shedding eddy. The length of the bar denotes the lifetime of the Kuroshio-shed eddy in the SCS, with the bottom and top of the bar representing the eddy shedding time and its demise time, respectively. The two dashed lines correspond to January 1 and May 1.

Figure 3 shows the relationship between the eddy strength and eddy lifetime. The eddy amplitude at the shedding moment ranges from 6 cm to 44 cm, with a mean amplitude of 19 cm. Their lifetime in the SCS varies from several weeks to months (24-257 days), with a mean lifetime of 89 days. The eddy lifetime exhibits a good linear relationship with the eddy strength at the shedding moment ($r = 0.72$), suggesting that stronger eddies tend to persist longer in the SCS. Stronger eddies possess more energy, resulting in longer persistence under similar environmental conditions, consistent with previous studies (Xiu et al., 2010). Notably, two strong and long-lived Kuroshio-shed eddies were observed in 2017 and 2021, exhibiting exceptionally strong magnitudes and long lifetimes that significantly deviate from the statistical means, nearly twice the standard deviation. Additionally, the eddy in 2010 was also

strong and persisted for more than 180 days. All three eddies re-intensified during summer, contributing to their prolonged lifespans in the SCS (Fig. 2).

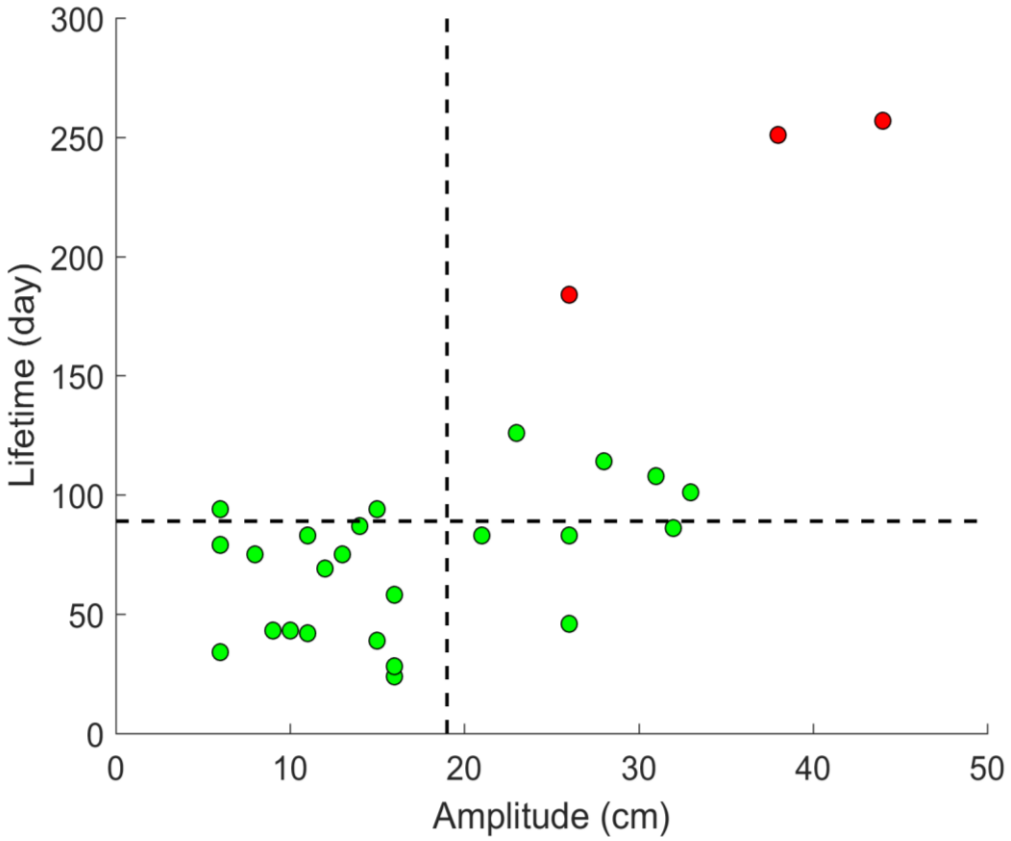

FIG. 3. Relationship between the strength and lifetime of Kuroshio anticyclonic eddies in the SCS. The dashed lines represent the mean amplitude and mean lifetime of the eddies. The three strong and long-lived shed eddies in 2010, 2017 and 2021 are marked by red dots.

The trajectories of the eddies show that, after shedding from the KLC, the anticyclonic eddies propagate southwestward to the interior SCS, basically along the isobaths of 1000-2000 m (Fig. 4). The propagation distance can reach 1000 km until the eddies finally dissipate near the Xisha Islands. Most of them (22/27) moved to the region south of 20°N and west of 116°E. The remaining eddies (5/27) dissipate near the Dongsha Islands. The dissipation of the eddies may have a potential impact on the local heat-salt balance and vertical mixing (Yang et al., 2019; Yang et al., 2021). Specifically, the trajectories of the strong long-lived eddies in 2010, 2017, and 2021 exhibited circular movement near the Xisha and Zhongsha Islands, which may be related to their re-intensification processes.

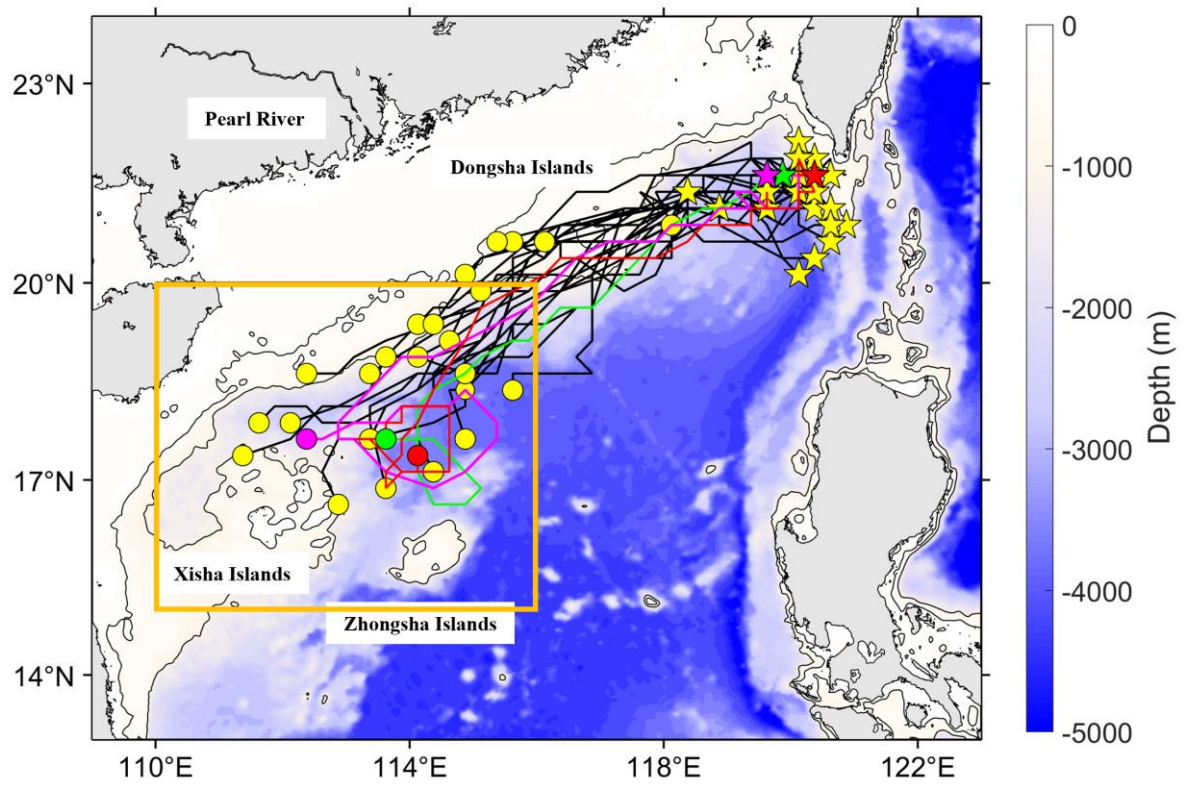

FIG. 4. Tracks of 27 Kuroshio anticyclonic eddies during 1993–2023. The star and circle represent the beginning and end of each eddy, respectively. The green, pink and red lines represent the eddy tracks observed in 2010, 2017 and 2021, respectively. Gray contours represent the 200-m and 1000-m isobaths. The orange box (110°E-116°E, 15°E-20°N) indicates the region influenced by the Xisha and Zhongsha Islands.

b. Evolution of Strong and Long-Lived Kuroshio Eddies

To examine the evolution of these exceptionally long-lived Kuroshio eddies, time series of sea level anomaly (SLA) and surface geostrophic currents over their entire lifespans are presented in Figures 5–7. The eddies in 2010, 2017, and 2021 exhibited similar development processes. They all generated in the Kuroshio loop current in the northeastern SCS during the late autumn of the preceding year and subsequently shed into the SCS in January 2010, February 2017, and March 2021, respectively. The amplitudes of the shedding eddies in 2017 and 2021 were 38 cm and 44 cm, respectively, making them the strongest Kuroshio-shed eddies ever recorded. In contrast, the shedding eddy in 2010 had a shorter development period, resulting in an amplitude of 26 cm when it was detached from the KLC. The shedding eddies moved southward along the continental slope with a mean propagation speed of 8.5 cm/s, reaching the Xisha Islands after approximately three months. This propagation speed is slightly higher than the phase speed of 7.1 cm/s for a free long Rossby wave of the first baroclinic mode

in the SCS (Yuan et al., 2007), as the SCS background current in winter is conducive to the southwestward propagation of the eddy.

After detachment from the KLC, the shedding eddies weakened continuously over time due to the loss of a steady energy supply. Note that the SLA at the centers of these three eddies rapidly decreased after April 10, 2010, May 22, 2017, and May 29, 2021, indicating that the topography of the Xisha Islands exerts a strong dissipative effect on the mesoscale eddies (Figs. 5g, 6g, and 7g). Statistical analysis shows that most of the Kuroshio eddies dissipate rapidly after passing through the Dongsha Islands or encountering the Xisha Islands (Fig. 4; Zhang et al., 2016; Yang et al., 2019). However, for these three long-lived eddies, despite their weakening, they consistently maintained a closed SLA contour (streamline) structure, with amplitudes greater than 2 cm (Figs. 5d, 6d and 7d). Moreover, after encountering and being obstructed by the Xisha Islands, these eddies turned eastward along the topography and re-intensified during summer. Once they drifted away from the islands, they moved westward again under the influence of the β effect. Ultimately, the Kuroshio-shed eddy in 2010 was absorbed by a larger anticyclonic eddy located southwest of Xisha Islands in mid-July 2010 (Fig. 5f). This event was documented by Chu et al. (2014), who reported that the merger of the two eddies resulted in one of the strongest anticyclonic eddies ever observed in the western SCS. However, their observational results indicated that the newly merged eddy no longer retained the high-salinity characteristics of Kuroshio water, instead exhibiting properties of typical SCS water. Therefore, we conclude that the original Kuroshio eddy had dissipated through merger. In contrast, the Kuroshio eddies in the other two years persisted until October 2017 and November 2021, respectively, and eventually dissipated near the Xisha Islands due to topographic effects (Figs. 6f and 7f). The Kuroshio eddy in 2010 persisted for 184 days, while the eddies in 2017 and 2021 lasted over 250 days after shedding from the Kuroshio, far longer than those regular Kuroshio-shed eddies (Fig. 3).

Details of SLA evolution during the eddy re-intensification stage suggest that eddy-eddy interactions may play a key role in the re-intensification of Kuroshio eddies in 2010, 2017 and 2021 (Figs 5h-j, 6h-j and 7h-j). During their eastward movement after being blocked by the Xisha Islands, the Kuroshio eddies encountered and interacted with another anticyclonic eddy from the eastern SCS. Initially, the two eddies were separated by a certain distance. As the Kuroshio eddy propagated eastward and the eastern eddy extended westward, they gradually approached and eventually merged. Following the merger, the Kuroshio eddy intensified rapidly, while the eastern eddy weakened, suggesting that the former absorbed energy from the

latter.

Oceanic eddies interact strongly with their surroundings rather than as isolated bodies of water. The merger of two like-signed coherent eddies, which results in the formation of a larger eddy, is an important mechanism for the intensification of mesoscale eddies (Trodahl et al., 2020; Wang et al., 2019). The process of eddy merging was especially pronounced in 2021, when the Kuroshio eddy nearly absorbed half of the eddy from the east, leading to its re-intensification (Fig. 7i). In contrast, the eddy merging in 2010 and 2017 were more like partial merger, manifested as the connection of the outer SLA contours (Figs. 5i and 6i). The energy from the eddy-eddy interactions seems insufficient to intensify the Kuroshio eddy to its final state (Figs. 5j and 6j). Instead, a northward current persisted on the western side of the Kuroshio eddy during its re-intensification process, which was most evident in both 2010 and 2017. This northward current originates from the summer SCS western boundary current, and, under the influence of a strong anticyclonic eddy in the southwestern SCS, it turned eastward around 14°N and then flowed northward through the narrow strait between the Xisha and Zhongsha Islands. Therefore, eddy-current interactions may be another mechanism driving the re-intensification of Kuroshio eddies in the summer.

Satellite observations can only provide sea surface information. To investigate the vertical structure of the Kuroshio-shed eddies, as well as the detailed processes of eddy merging and re-intensification mechanisms, in-situ observations and reanalysis data were utilized in the following sections.

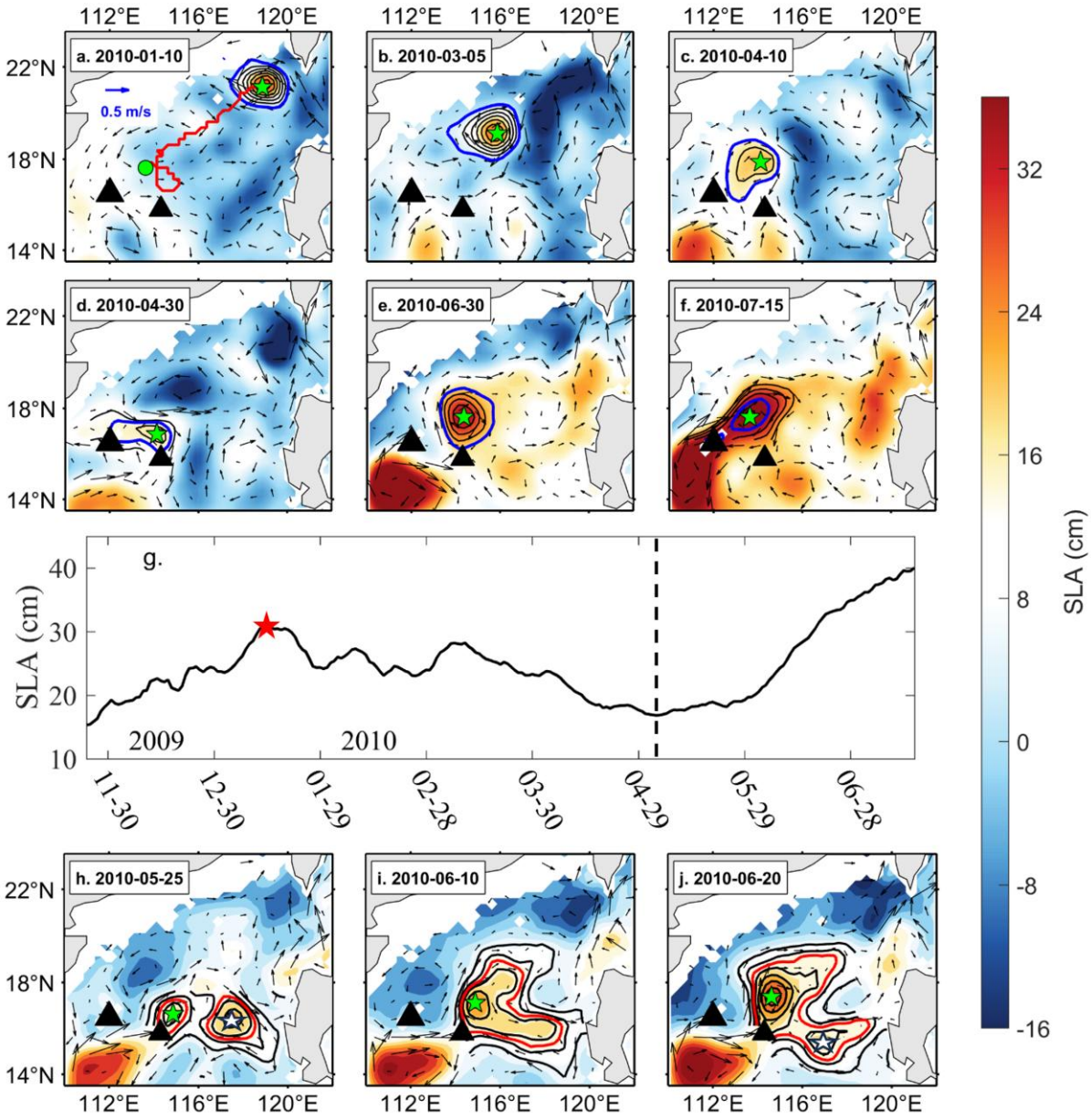

FIG. 5. (a)–(f) Maps of the SLA (shading; cm) and surface geostrophic current (vectors; m/s) from January 2010 to July 2010. Regions shallower than 100 m were masked by white shading. Green star and blue contour represent the center and edge of the Kuroshio anticyclonic eddy. Black contours denote the SLA with 4-cm intervals within the eddy. The black triangles indicate the Xisha and Zhongsha Islands. The red line and green dot in panel (a) represent the eddy trajectory and its demise location, respectively. Note that to highlight the structure of the Kuroshio eddy, the color bar here is not symmetrically centered around zero. (g) Time series of SLA at the eddy center. The red star and the black dashed line indicate the eddy shedding and its weakest moment, respectively. (h)–(j) Detailed evolution of SLA and surface geostrophic current during eddy's re-intensification process. Green and white stars indicate the center of Kuroshio eddy and the SCS eddy from the east, respectively. Black contours denote the SLA with 4-cm interval and the red contour is the 15-cm SLA.

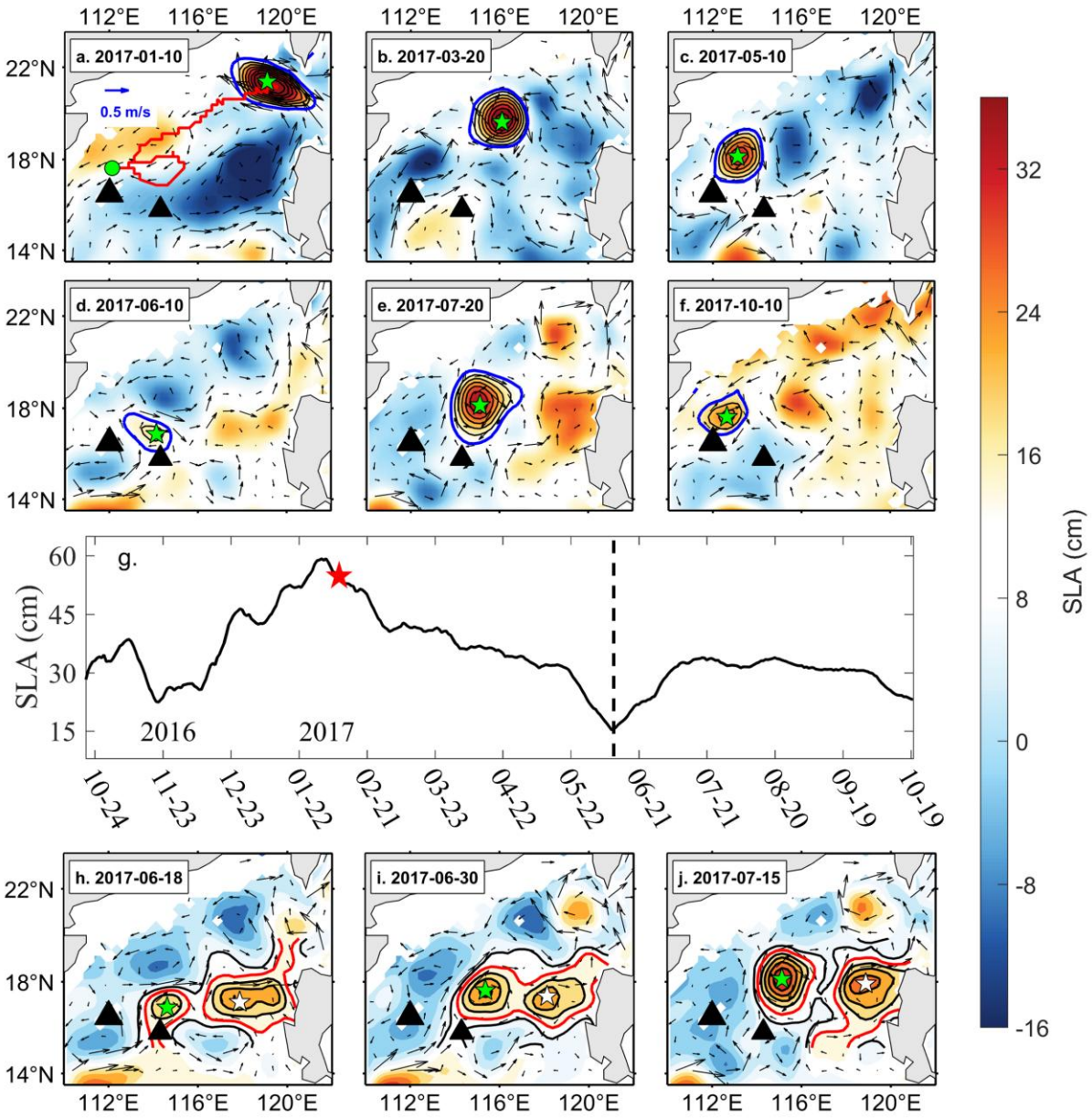

FIG. 6. Similar to Figure 5, but for the Kuroshio eddy in 2017. The red contour in (h)–(j) denotes the 14-cm SLA.

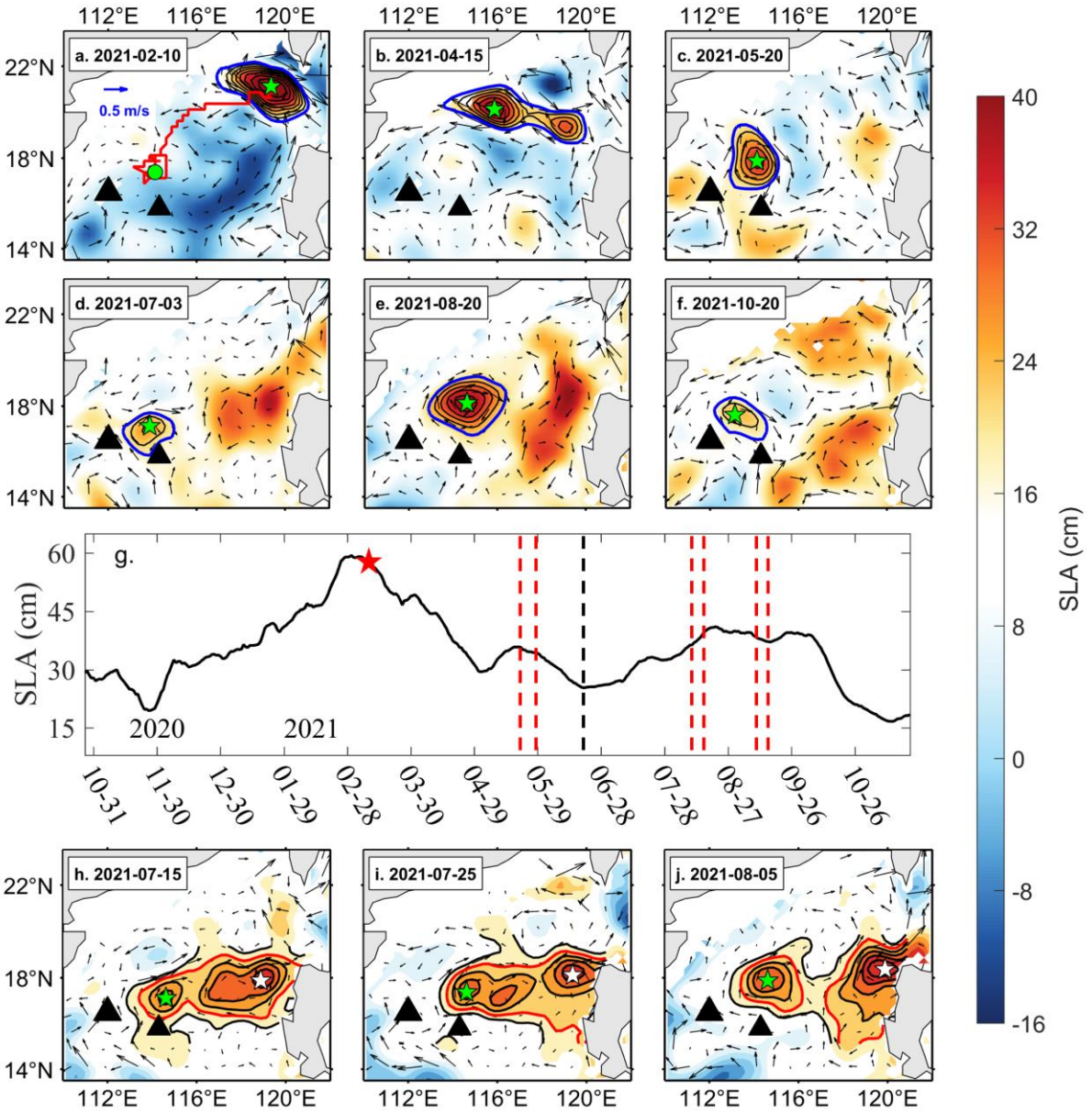

FIG. 7. Similar to Figure 5, but for the Kuroshio eddy in 2021. The red dashed lines in (g) indicate the time of three cruise observations. The red contour in (h)–(j) denotes the 22-cm SLA.

c. Hydrographic Observations in 2021

Argo float and three targeted cruise observations in 2021 provide an opportunity to examine the evolution of eddy's vertical structure and water mass characteristics (Fig. 1). Figure 8 shows the vertical distributions of temperature, salinity, and PV and Rossby number at different stages of the Kuroshio eddy. Here, we only present the observational results from Argo profiles and cruise transects B, C, and F, as the results from the other three transects are quite similar (Fig. S1). In December 2020 and January 2021, the Argo float observed two intense high-salinity events, with salinity exceeding 34.8 psu. These events were attributed to

the robust intrusion of the KLC and the westward advection of saltier Kuroshio water during this period, as the Argo float was situated in the edge of the eddy (not shown). Subsequently, as the anticyclonic eddy gradually separated from the Kuroshio, the Argo float entered the eddy's interior, enabling it to observe the distinct water properties within the eddy. From Argo observations (Fig. 8a, e, i), it is evident that the main thermocline (halocline/pycnocline) deepens inside the anticyclonic eddy, exhibiting a typical surface-intensified vertical structure and a thick body of low temperature and high salinity water. The maximum salinity within the eddy was found at about 220 m, much deeper than that outside (~150 m). The water inside the eddy was characterized by low PV, which was related to the deepening of the mixed layer caused by the strong convective mixing in winter and the downward movement of the pycnocline inside the anticyclonic eddy.

After shedding from the Kuroshio, the anticyclonic eddy propagated southwestward to the interior SCS and was observed by three successive cruise surveys in May, August, and September 2021. Interestingly, the eddy exhibited a lens-shaped vertical structure in the upper 300 m at all three stages, significantly different from the general vertical structure of surface-intensified anticyclonic eddy. The lenticular body, composed of low PV water, depressed the lower thermocline (halocline/pycnocline) but raised the upper thermocline (halocline/pycnocline). These features are typical characteristics of a subsurface-intensified anticyclonic eddy, implying that the Kuroshio eddy had evolved from a surface-intensified eddy to a subsurface-intensified eddy. The horizontal scale of the lens core was approximately 120 km, with the Rossby number in the eddy core ranging from –0.5 to –0.8, confirming the significant role of nonlinear inertial forces in the Kuroshio eddy dynamics. The high PV at the edges of the lens core acts as a barrier, preventing the exchange of water between the eddy core and the surrounding waters. From May to September, the subsurface lens-shaped structure and the water mass properties trapped inside the eddy core were preserved well even after experiencing topographic dissipation and merging with another anticyclonic eddy from the eastern SCS. This result indicates that the Kuroshio eddy dominated the eddy merging process in summer, and the subsurface lens-shaped structure exhibits good conservative characteristics.

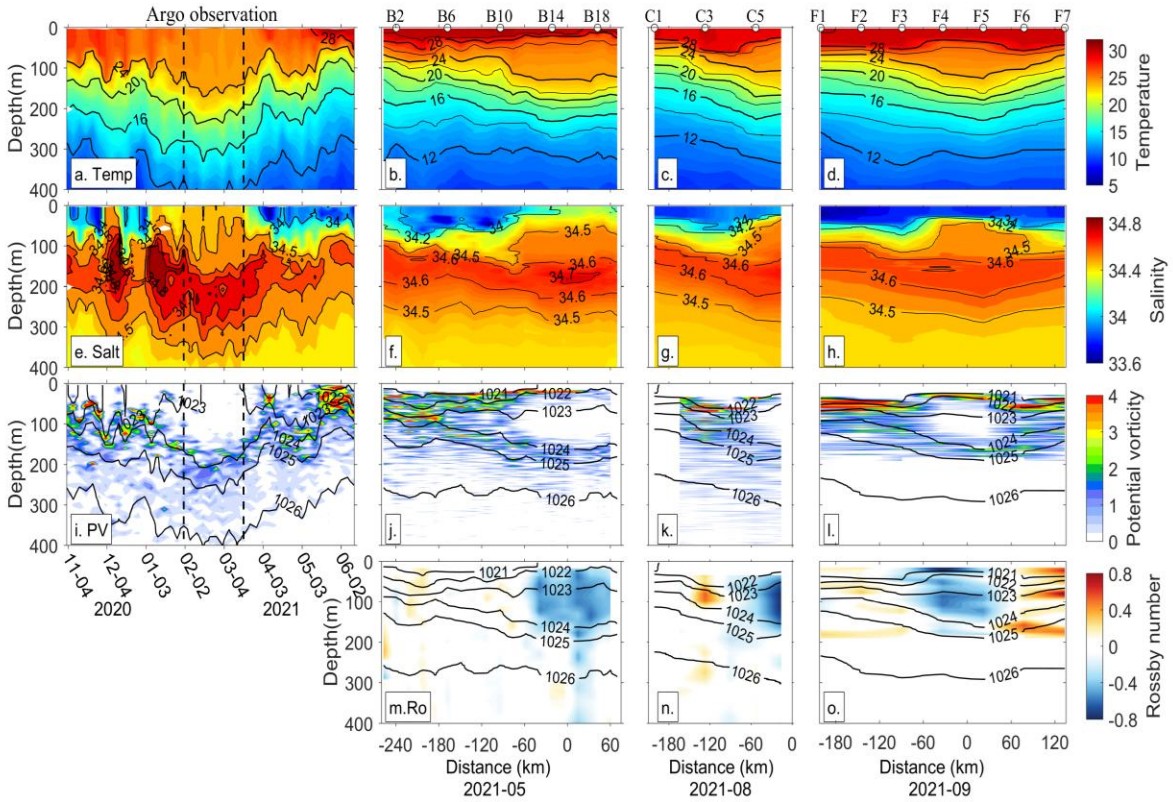

FIG. 8. Hydrographic observations at different stages. (a)-(d) Temperature (°C). (e)-(h) salinity (psu). (i)-(l) Potential vorticity (PV; 10^{-9} $m^{-1}s^{-1}$). (m)-(o) Rossby number (Ro). From left to right, the columns are Argo and cruise observations in May, August, and September 2021, respectively. The dashed black lines in the left column denote the Argo observation inside the eddy from February 1 to March 19, 2021. Black lines in PV panels represent isopycnals. The zero point on the x-axis represents the eddy center.

Figure 9 presents the vertical distribution of horizontal velocities observed by shipboard ADCP in May and September 2021. The eddy exhibited a subsurface-intensified structure, corresponding to its vertical lens-shaped structure. The subsurface core was located above 200 m, with a maximum velocity exceeding 0.6 m/s observed at ~85 m. Note that the distribution of the lens-shaped structure did not entirely match the range of the anticyclonic eddy observed by satellite altimetry (Figs. 1 and 9). It was only contained within the core portion of the anticyclonic eddy, while the rest remained as a traditional surface-intensified structure. Although satellite observations show that the eddy decayed rapidly with relatively low SLA and a small eddy area in June 2021 after encountering the Xisha Islands, the core part of the eddy was still remained (Fig. 7d). Based on the low PV and the velocity maximum structure, a threshold of 0.5 cm/s can be defined as the horizontal boundary of the lens-shaped core, within which the water properties are well preserved. Using this criterion, the horizontal scales of the lens-shaped structure can be estimated, as illustrated in Figure 1b and 1d. In May, the

horizontal extent of the lens-shaped structure was 115 km (113.5°E–114.5°E) and 154 km (16.7°N–18.0°N) in transects A and B, respectively. After interacting with the topography and the surrounding environment, the Kuroshio eddy underwent deformation, with the meridional radius contracting and the zonal radius stretching (Fig. 7). In September, the horizontal extent of the lens-shaped structure was 138 km (113.8°E–115.1°E) and 122 km (17.1°N–18.2°N) in transects E and F, respectively.

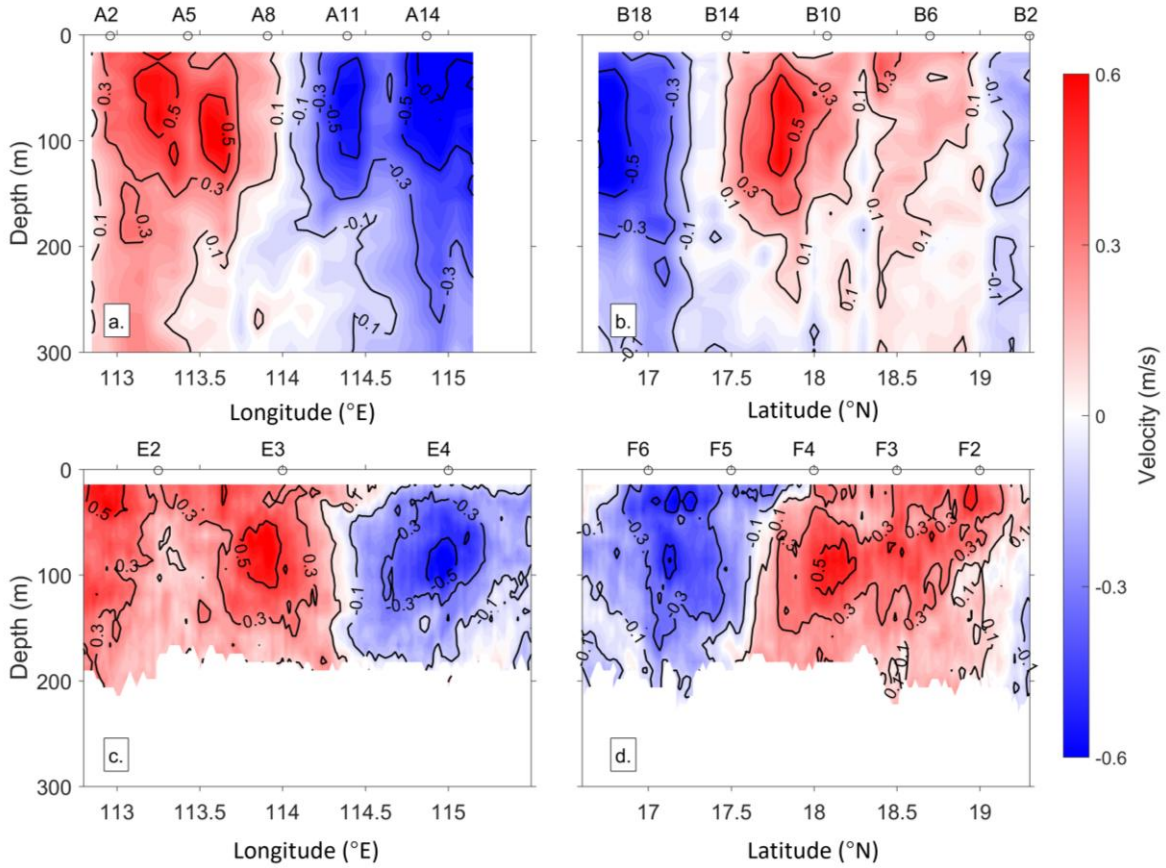

FIG. 9. Horizontal velocity (m/s) observed by shipboard ADCP. (a)-(b) Cruise observation in May 2021. (c)-(d) Cruise observation in September 2021. The velocity shown here is perpendicular to the transect.

To analyze the changes in water mass properties trapped in the eddy, we plotted the *T*–*S* diagrams of the shed eddy at different life stages (Fig. 10). The Kuroshio water is warmer and saltier than the SCS water in the upper layer (>26 σ_θ) but colder and fresher in the intermediate layer (26-27.5 σ_θ). The water within the eddy shows characteristics between the Kuroshio water and SCS water above 25.6 σ_θ, while below this depth, it resembles the northern SCS water (Fig. 10d). This result suggests that the high-salinity water trapped in the eddy was a mixture of Kuroshio and northern SCS water, and the Kuroshio water intrusion was primarily confined to the upper 25.6 σ_θ layer. With high-resolution (~15 km) CTD station observations

in May, a noticeable transition in water characteristics can be observed from the core, through the edge, and to the exterior of the lenticular body (Fig. 10b). The observations in August and September both represent the stages of eddy re-intensification, with relatively similar water characteristics. From March to September, the water properties within the eddy center gradually changed, yet they still exhibited distinct differences from the surrounding water. Specifically, the salinity within the eddy gradually decreased in the lower part of the lens-shaped structure (23.2-25.6 σ_θ), whereas in the upper part of the lens-shaped structure (22-23.2 σ_θ), the salinity gradually increased (Fig. 10d). This trend may be related to the intensified vertical mixing induced by the drastic changes in eddy intensity.

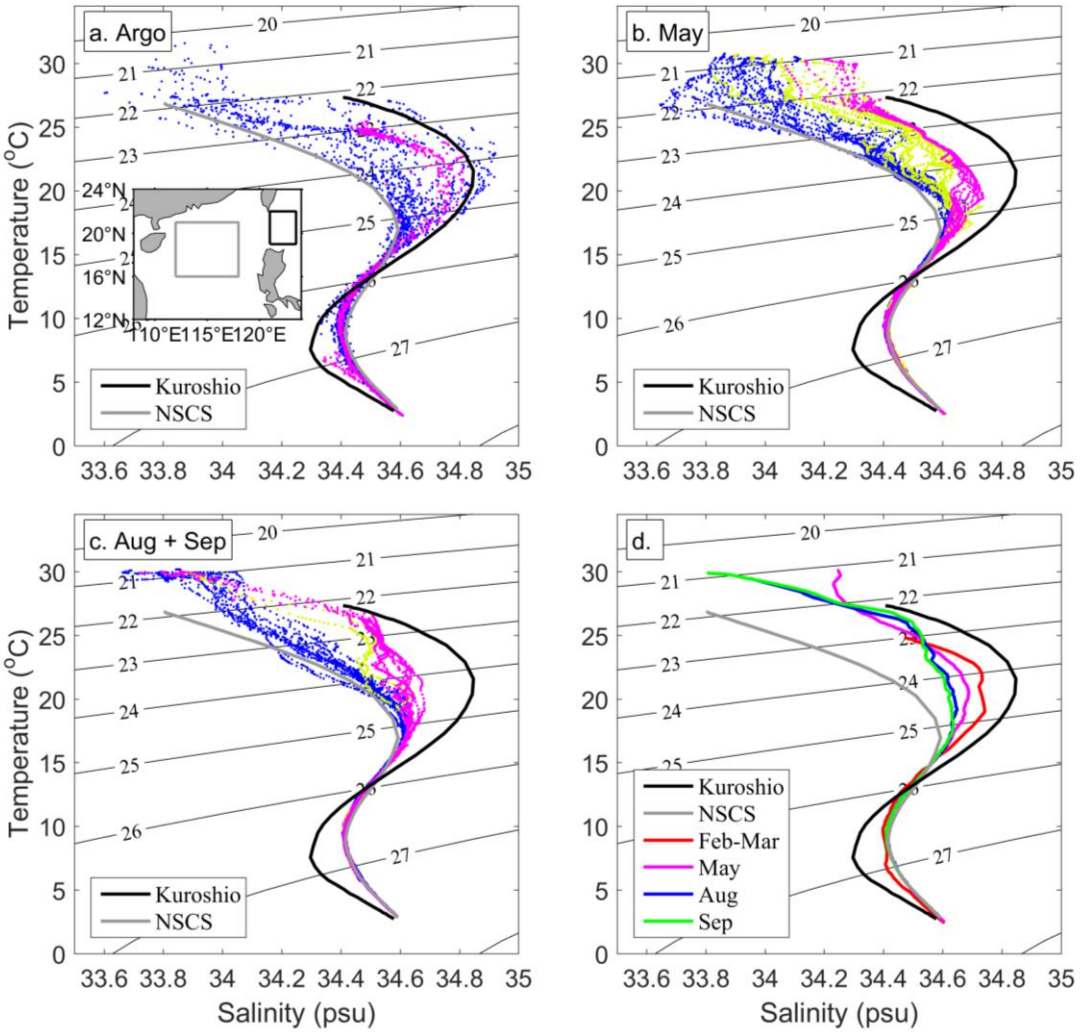

FIG. 10. *T–S* diagrams from Argo and cruise observations. (a) Argo observations from November 2020 to June 2021. (b) Cruise observations in May 2021. (c) Cruise observations in August and September 2021. (d) The mean *T-S* curves within the eddy at different stages. Black and gray lines indicate the basic characteristics of Kuroshio water (black box in the inset) and northern SCS water (NSCS, gray box in the inset), respectively, based on *WOA18* climatology data. Pink and blue dots in (a) show the *T/S* data inside and outside the eddy. Pink, yellow, and blue dots in (b) and (c) show the water properties in the core (see the

pink dots in Fig. 1), at the edge (see the white dots in Fig. 1), and outside (see the green dots in Fig. 1) of the lens-shaped structure, respectively. The red line in (d) represents the mean *T-S* curve within the eddy observed by the Argo float. The pink, blue, and green lines in (d) represent the mean *T-S* curves within the lens core.

Since the anticyclonic eddy shed from the KLC and ultimately dissipated near the Xisha Islands, it is instructive to estimate how much the shed eddy transported Kuroshio water to the interior SCS. If we only consider isopycnal mixing, the percentage of Kuroshio water, denoted as a, trapped within the eddy can be generally estimated, using $S_{AE} = aS_{Kur} + (1-a)S_{SCS}$, where S_{AE}, S_{Kur} and S_{SCS} denote the salinity of the shed eddy, Kuroshio, and northern SCS water, respectively. The basic characteristics of Kuroshio water and SCS water were obtained from *WOA18* climatology data. The water properties trapped in the eddy were obtained from Argo float and CTD observations, respectively. Substituting the salinities in Figure 10d into this formula, the percentages of eddy-trapped Kuroshio water on each isopycnic surface were obtained. Therefore, the proportion of Kuroshio water within the eddy core (22 σ_θ −25.6 σ_θ) was found to be 62% in March, 56% in May, and 48% in September. The proportion of Kuroshio water slightly changed from March to September, indicating that water characteristics within the eddy core were generally well maintained.

With some reasonable assumptions, the volume of Kuroshio water trapped in the eddy core can be estimated. Assuming that the lens-shaped structure observed in May was an irregular elliptical cylinder, with transect A serving as the base and oriented horizontally along the transect B (Fig. 1b). The base area of the lenticular body in transect A (within 22-25.6 σ_θ) was estimated to be about 2.22 x 10^7 m^2. By multiplying the height of the cylinder in transect B (154 km), the volume of the lens-shaped structure was obtained to be ~3.42 x 10^{12} m^3. Considering the proportion of Kuroshio water within the eddy, the Kuroshio water trapped in the lens-shaped structure was estimated to be ~1.91 x 10^{12} m^3. Similarly, in September, the Kuroshio water trapped in the lens-shaped structure was estimated to be about 1.45 x 10^{12} m^3. Notably, these volumes are nearly 4-5 times the annual discharge of the Pearl River into the SCS (3.6×10^{11} m^3; Sheng et al., 2023). This suggests that the shed eddy transported a substantial amount of warm, saline, and oligotrophic Kuroshio water to the Xisha Islands, potentially influencing the local heat-salt balance and ecological processes.

d. Mechanisms of eddy re-intensification

To understand the dynamics of eddy re-intensification, we utilized eddy-resolving

reanalysis data to examine the detailed processes of eddy merging in 2010, 2017 and 2021. The 3D structure of the eddies from the CMEMS reanalysis data shows that the Kuroshio eddy was a subsurface-intensified eddy with a core that traps higher-salinity water (Fig. 11). During the re-intensification process, the water properties in the eddy core remained largely unchanged, a characteristic most evident in 2017 and 2021, consistent with hydrographic observations (Fig. 8; Sun et al., 2022). In contrast, the eddy in 2010 was significantly weakened after interacting with the topography of Xisha and Zhongsha Islands. As a result, the conservative properties of the eddy core were less well maintained, leading to a decrease in its core salinity after re-intensification. Nevertheless, the eddy core at 50 m and 100 m depths still retained certain high-salinity characteristics of Kuroshio water. From the distribution of salinity, it can be inferred that the low-salinity water wrapped around the periphery of the Kuroshio eddy likely originated from the anticyclonic eddy to its east or from the southwestern SCS advected by a northward flow.

Relative vorticity and the horizontal gradient of PV can be used to characterize the intensity of the eddy as well as the strength of water exchange between the eddy core and its surroundings (Bosse et al., 2019; Trodahl et al., 2020). Figures 12–14 demonstrate the evolution of the Kuroshio eddies and their interactions with the surrounding currents and eddies. During the summer of 2010, from May 1 to May 22, as the Kuroshio eddy moved eastward, it weakened rapidly due to dissipation caused by the island topography. Afterward, driven by the background current, the eddy moved northward, away from the Zhongsha Islands. The eddy's intensity remained relatively stable from May 23 to June 4. After that, the eddy intensified rapidly, reaching its peak strength around June 30. The horizontal distribution of relative vorticity suggests that the negative vorticity associated with the eddy's re-intensification originated from a northward current on its west side and an anticyclonic eddy to its southeast. The northward current originates from the summer SCS western boundary current. Induced by a strong anticyclonic eddy in the southwestern SCS, the northward western boundary current turned eastward around 14°N, then shifted northward at approximately 113°E, flowing through the narrow strait between the Xisha and Zhongsha Islands (Fig. 12a). Due to the current-topography interactions, strong negative relative vorticity was continuously generated west of the Zhongsha Islands. As time progressed, the negative vorticity was gradually advected toward the Kuroshio eddy region, where it was entrained by the eddy (Figs. 12b-e). Additionally, between June 10 and June 30, the Kuroshio eddy interacted with an anticyclonic eddy to its southeast, which also supplied negative vorticity to the Kuroshio eddy (Figs. 12c-e). This

sustained input of negative vorticity contributed to the eddy's re-intensification, as evidenced by a noticeable increase in both radius and amplitude. Both eddy-current and eddy-eddy interactions played significant roles in the re-intensification of the Kuroshio eddy in 2010. This result is consistent with satellite observations (Figs. 5 and 12). Moreover, we analyzed the distribution of the horizontal PV gradient around the eddy to assess the water exchange between the eddy core and its surroundings (Figs. 12h-j). The results show that during the early stage, the eddy core was enclosed by a ring of high PV gradient, which inhibited water exchange between the interior and exterior of the eddy. However, over time, the PV gradient weakened and the closed structure dissolved, allowing the high-salinity water in the eddy core to mix with the surrounding low-salinity water. Consequently, the salinity within the eddy core decreased following re-intensification (Figs. 11a-c).

The re-intensification process of the Kuroshio eddy in the summer of 2017 resembled that in 2010 (Fig. 13). A northward current on the eddy's west side continuously advected negative vorticity – generated west of the Zhongsha Islands – into the eddy region, where it was eventually entrained and absorbed by the Kuroshio eddy, contributing to the eddy's intensification. It is worth noting that the interaction between the Kuroshio eddy and the anticyclonic eddy to its east is not clear evident from the reanalysis data. This may be due to the relatively large distance between the two eddies, with only partial merging occurring at their peripheries (Figs. 6h-j). Consequently, the reanalysis data may not fully capture the eddy-eddy interaction process. However, Fu et al. (2023) found that multi-core eddy structure and shared contours play a pivotal role as an intermediary phase in the merging process, facilitating significant exchange of energy and vorticity between the two eddies. The similar structure was observed in the case of 2017 (Fig. 6i), suggesting that eddy-eddy interactions may have also played an important role in the re-intensification of Kuroshio eddy in 2017.

Unlike the 2010 case, the Kuroshio eddy in 2017 exhibited pronounced subsurface-intensified structure. Although satellite altimeter data indicated a weaker sea surface signal, its core consistently maintained strong subsurface velocities (Figs. 11d-f). As a result, during the eddy's re-intensification, a nearly closed and strong PV gradient formed around its core, acting as a PV barrier that prevented water exchange between the eddy core and its surroundings (Figs. 13h-j). Consequently, the water properties within the eddy core were well-preserved.

Compared to the cases in 2010 and 2017, the re-intensification of the Kuroshio eddy in 2021 was primarily driven by its merger with an anticyclonic eddy to its east (Fig. 14). In this year, there was no strong northward flow on the western side of the Kuroshio eddy because the

anticyclonic eddy southwest of the Xisha Islands was relatively weak and located farther south, making it difficult to induce a northward current through the narrow strait between the Xisha and Zhongsha Islands. Instead, the Kuroshio-shed eddy underwent a clear merging process with the anticyclonic eddy to its east. Compared to the Kuroshio eddy, the eastern anticyclonic eddy was weaker. During their interactions, the eastern eddy was gradually disrupted by the Kuroshio eddy, becoming strongly elongated and eventually wrapped around the Kuroshio eddy (Figs. 14b–e). Although the relative vorticity at the core of the Kuroshio eddy remained largely unchanged, negative vorticity from the eastern eddy was incorporated into its periphery, which increased the eddy's radius and amplitude, ultimately leading to its re-intensification. Notably, during this period, the Kuroshio eddy core remained enclosed by a high PV gradient ring, which effectively inhibited the exchange of high-salinity core water with the low-salinity water at the eddy periphery (Figs. 14h-j). This explains why hydrographic observations recorded only slight changes in water properties after eddy re-intensification from May to September 2021 (Figs. 8 and 10).

By analyzing the three cases in 2010, 2017, and 2021, we found that both eddy-current and eddy-eddy interactions are primary mechanisms driving the summer re-intensification of long-lived Kuroshio eddies in the SCS (Fig. 15). In different years, these two mechanisms may coexist or operate independently. Additionally, the strong Kuroshio eddies form a closed high-value PV gradient around the eddy core, acting as a PV barrier that inhibited water exchange between the eddy's interior and its surroundings. Consequently, the absorbed water wraps around the eddy core, while the water properties within the core remain well preserved.

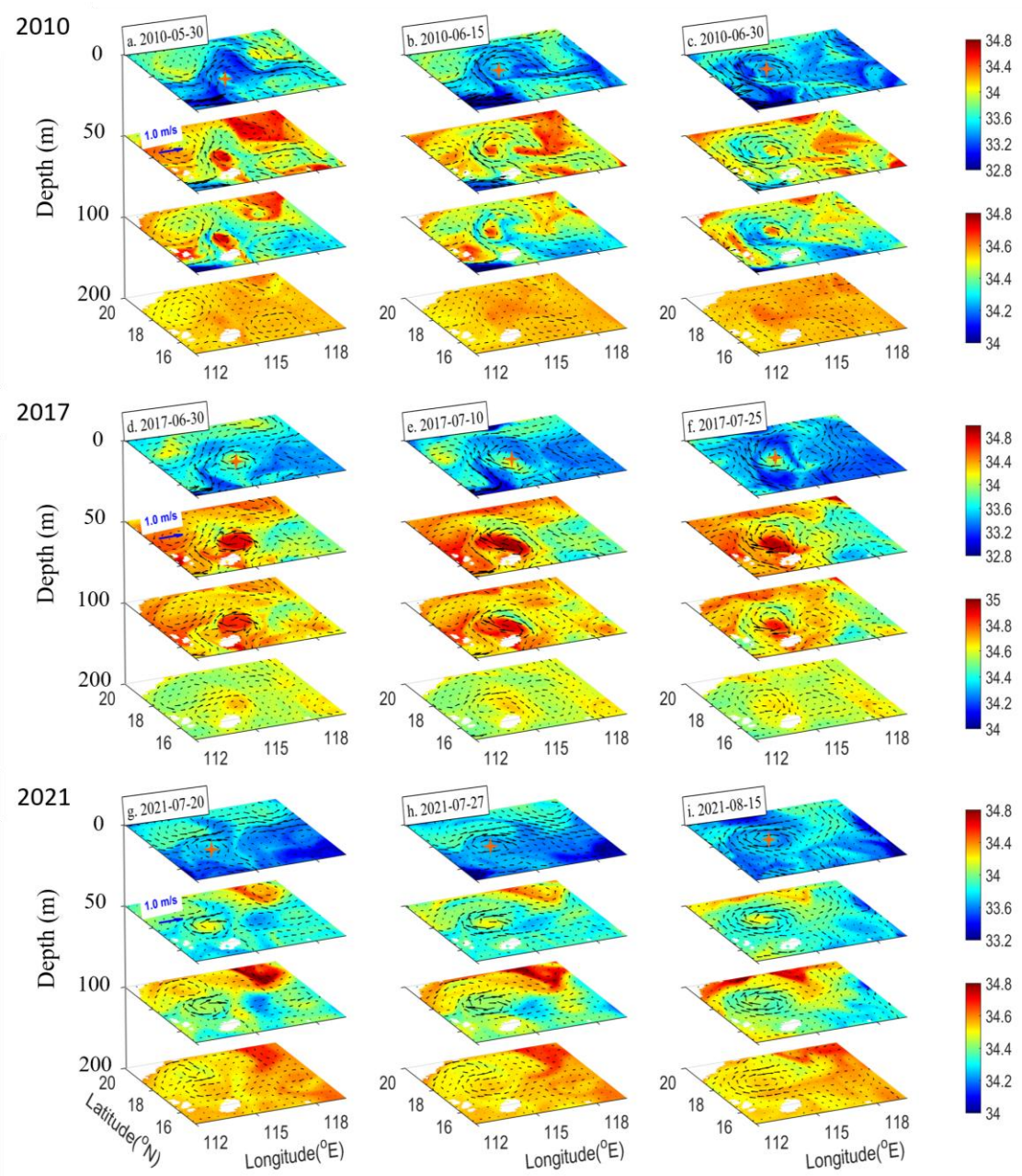

FIG. 11. Three-dimensional (3-D) structure of the oceanic eddies during their re-intensification processes. The top row (a-c), middle row (d-f), and bottom row (g-i) represent the eddy in 2010, 2017 and 2021, respectively. Shading and black arrows denote the salinity and velocity vectors (m/s), respectively. The orange cross represents the Kuroshio eddy center. Note that salinity at 0 m and 50 m, and at 100 m and 200 m, share the same colorbars, respectively.

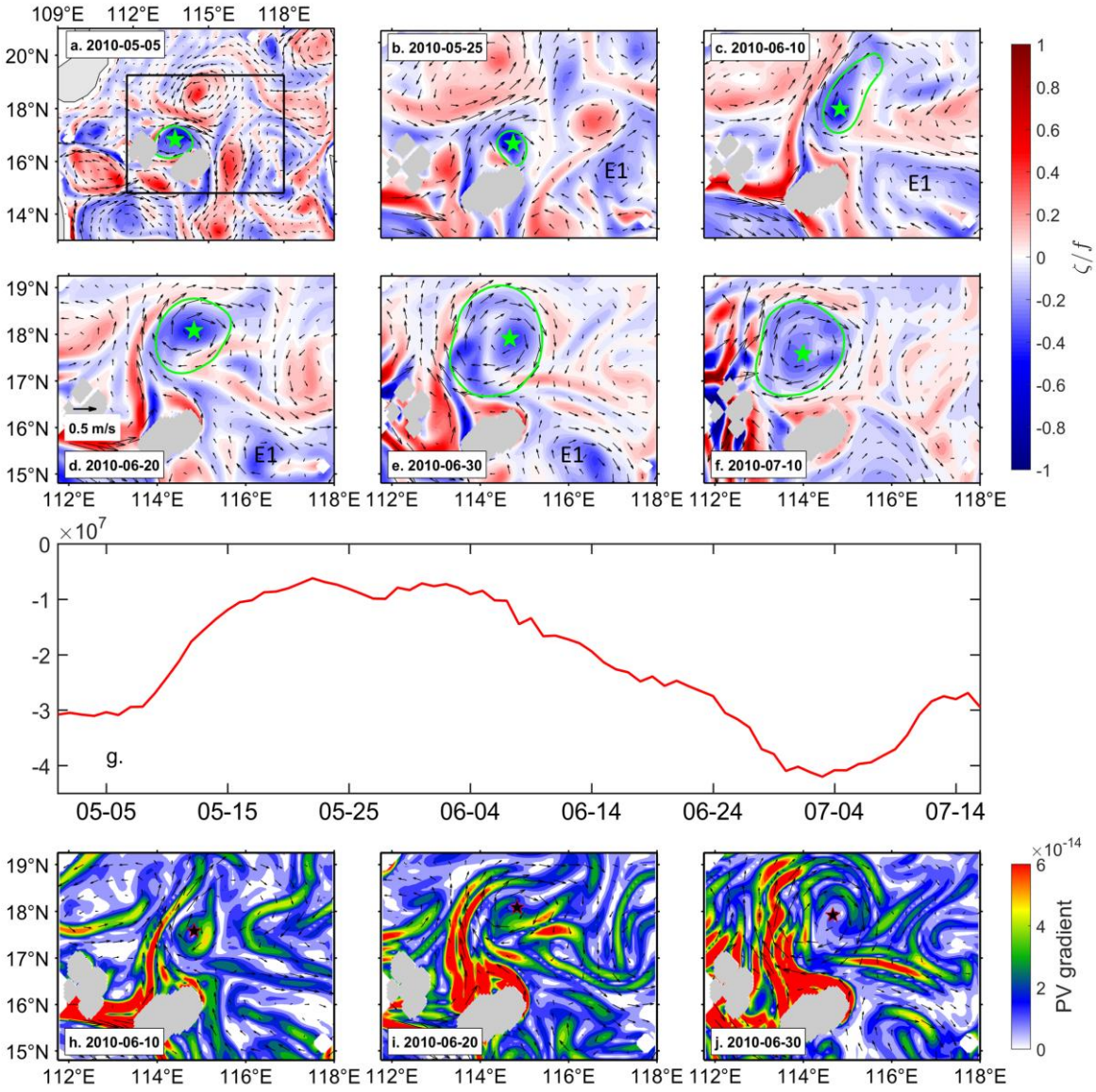

FIG. 12. (a)-(f) Horizontal maps of relative vorticity normalized by *f* at 50-m depth during the stage of eddy re-intensification in 2010. Black arrows denote the velocity vectors (m/s). Green star and line represent the center and edge of the Kuroshio eddy, respectively. The eddy to its east is denoted as E1. Black box in subplot (a) indicates the display range of subplots (b-f). The regions of Xisha and Zhongsha Islands are masked in gray. (g) Time evolution of the integrated negative relative vorticity within the eddy in upper 200 m. (h)-(j) Horizontal PV gradient ($m^{-2}\ s^{-1}$) at 50-m depth. The eddy center is marked by a black star.

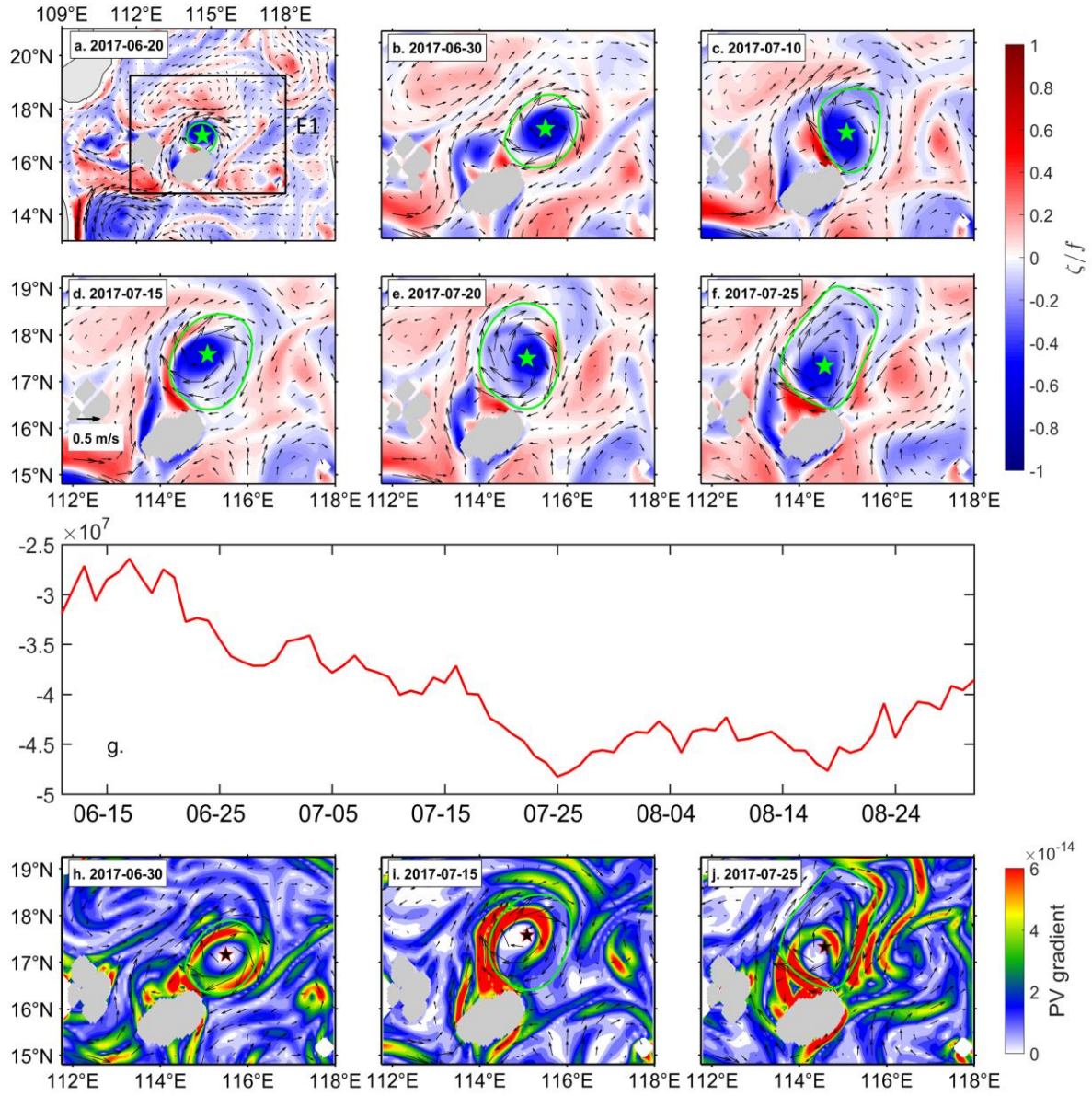

FIG. 13. Similar to Figure 12, but for the Kuroshio eddy in 2017.

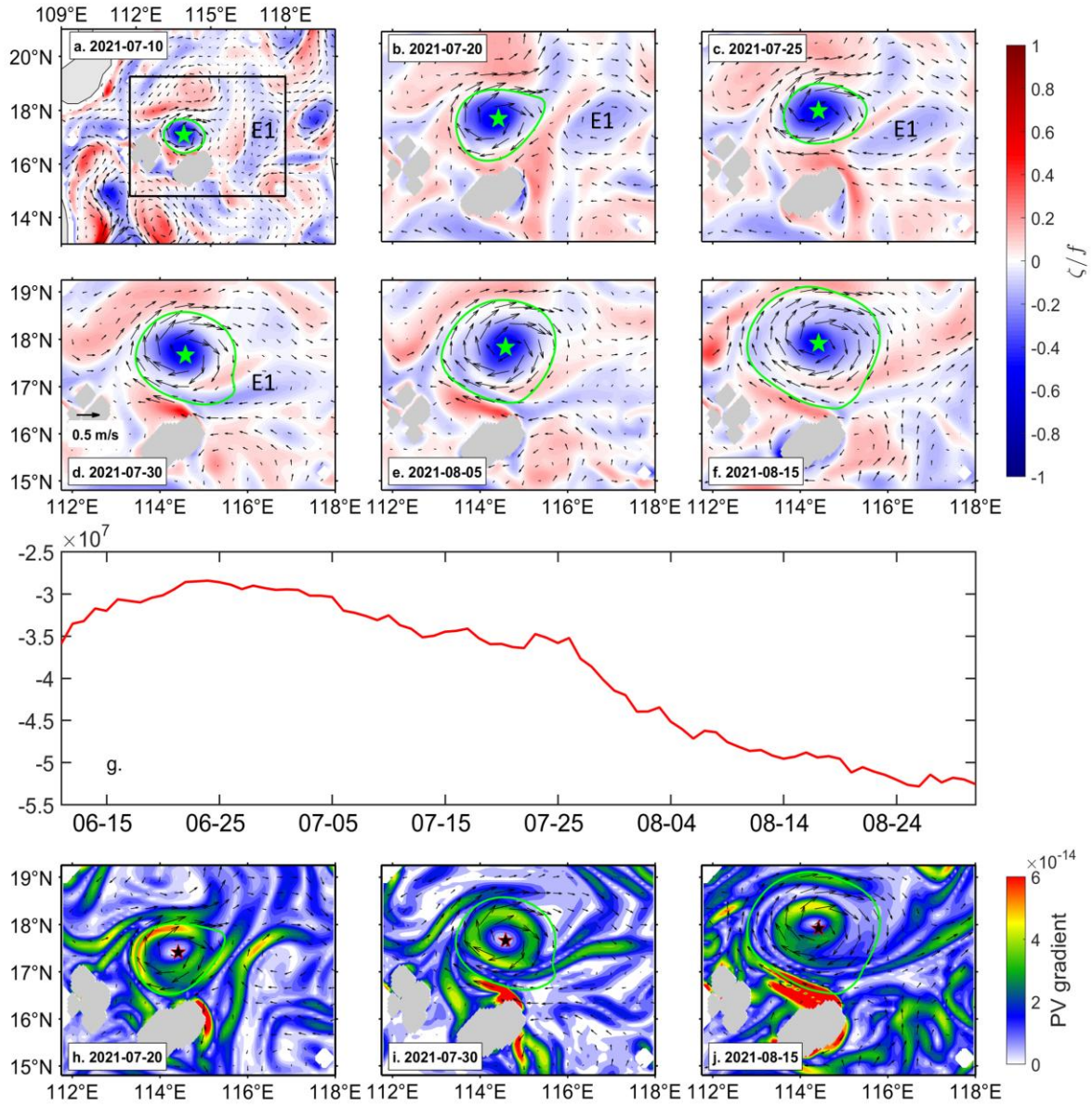

FIG. 14. Similar to Figure 12, but for the Kuroshio eddy in 2021.

4. Discussion

The Kuroshio-shed anticyclonic eddies in 2017 and 2021 are the two strongest and longest-lived eddies on record. Figure 2 shows that the frequency and intensity of the Kuroshio-shed eddies exhibit significant interannual and decadal variabilities. Sun et al. (2020) investigated the interannual variability of the KLC in the northeastern SCS. They found that the strength of the KLC is significantly modulated by ENSO, being stronger in La Niña and weaker in El Niño years. They also noted that the KLC event during the 2016/17 La Niña winter was the strongest observed between 1993 and 2019, primarily driven by enhanced wind work associated with a strengthened northeast monsoon. Additionally, both 2020 and 2021

were La Niña years. The intensified orographic negative wind stress curl southwest of Taiwan Island in the winter of 2020/21 contributed to the formation of a strong KLC (Sun et al., 2021). Since the anticyclonic eddies are generated within the KLC, the strength of the KLC significantly affects the intensity of the shed eddies. This finding helps explain the strong Kuroshio eddies observed in 2017 and 2021.

The present study found that strong Kuroshio eddies tend to have longer lifespans and may regain energy and re-intensify east of the Xisha islands during summer. In addition to the cases in 2010, 2017, and 2021, the Kuroshio eddies in 1995 and 2020 may have also undergone similar re-intensification processes (not shown). Due to the strong dissipative effects of the Xisha Islands, the SLA contours of these two eddies were not closed at certain stages. As a result, the re-strengthened eddies may have lost their Kuroshio water characteristics and were thus considered to have dissipated prior to re-intensification. However, these eddies are subsurface-intensified, meaning that while the surface eddy structure may have been disrupted, a closed subsurface structure could still be maintained. The re-intensification of the Kuroshio eddies in the northern SCS is likely a common seasonal phenomenon, phase-locked and synchronized with the development of eddies and circulation adjustments in the region during summer. Although many Kuroshio eddies can move to the Xisha and Zhongsha Islands region, most of them dissipate by spring and thus do not persist long enough to encounter the favorable background conditions necessary for intensification. Chu et al. (2020) found that the periodic eddies in the SCS exhibit an inverse “L” shape eddy train structure along the western boundary and around the 17°N section, with an anticyclonic phase in summer and a cyclonic phase in winter. The Kuroshio eddy, upon reaching the Xisha Islands, is influenced by this “L” shape system. Consequently, it is more likely to gain energy from this large system during summer, leading to its re-intensification.

Previous studies have demonstrated that mesoscale eddies have profound effects on heat and salt transport (Dong et al., 2014), chlorophyll distribution (He et al., 2016), primary productivity (Gaube et al., 2013), and air-sea heat flux (Leyba et al., 2017). The Kuroshio eddies can transport substantial amounts of Kuroshio water, along with distinct physical and biological properties, to the interior SCS, potentially exerting significant influence on the local heat-salt balance and marine ecosystem structure (Yang et al., 2021; Sun et al., 2022). The strong long-lived Kuroshio eddies exhibit a subsurface lens-shaped structure, with a shoaling of the seasonal thermocline and deepening of the main thermocline. The uplift of the seasonal thermocline may bring nutrients from deeper layers into the euphotic zone, thereby enhancing

primary production (McGillicuddy 2016). Moreover, the Kuroshio anticyclonic eddies exhibit a cold-core structure in the upper layer, which may influence air-sea interaction differently from conventional warm-core anticyclonic eddies (Ni et al., 2021; Wang et al., 2023). These aspects are beyond the scope of the present study and warrant further investigation in future work.

5. Conclusions

The Kuroshio intrusion and its associated anticyclonic eddy shedding are important oceanic dynamic processes in the northeastern SCS. Using satellite and in-situ observations together with reanalysis data, this study examined the characteristics of the Kuroshio-shed anticyclonic eddies, in particular, focusing on the evolution of three strong and long-lived eddies observed in 2010, 2017, and 2021. From 1993 to 2023, 27 prominent Kuroshio anticyclonic eddies were identified based on 31-year historical satellite altimeter data. Typically, these eddies shed from the KLC during winter, then propagate southwestward along the continental slope, with most dissipating by the following spring near the Xisha Islands. The eddy lifespans exhibit a good linear relationship with their shedding amplitudes, suggesting that stronger Kuroshio eddies tend to persist longer in the SCS.

The Kuroshio anticyclonic eddies in 2010, 2017, and 2021 are the three longest-lasting eddies on record. Unlike the regular Kuroshio eddies that dissipated upon encountering the Xisha Islands, these long-lived shed eddies slightly moved eastward along the island topography and re-intensified during the summer, persisting for more than 180 days in the SCS. Hydrographic observations in 2021 revealed that the long-lived Kuroshio eddy transformed from a surface-intensified to a subsurface-intensified eddy with seasonal changes, ultimately exhibiting a lens-shaped vertical structure in the upper 300 m. From May to September 2021, despite undergoing dissipation and merging, the Kuroshio eddy maintained its vertical lens-shaped structure and preserved high-salinity and low-PV water within the eddy core. The volume of Kuroshio water trapped in the eddy core was estimated to be 4 to 5 times the annual discharge of the Pearl River to the SCS.

Further analysis revealed that eddy-current and eddy-eddy interactions are the two main mechanisms driving the re-intensification of Kuroshio eddies in the SCS (Fig. 15). The long-lived eddies re-intensify either by absorbing negative vorticity advected from a northward current on their western side, generated by current-topography interactions, or by merging with an anticyclonic eddy to the east. These mechanisms can coexist or operate independently,

depending on the year. Strong Kuroshio eddies are encircled by a closed high-PV gradient ring, which acts as a barrier to water exchange, thereby preserving the core water properties.

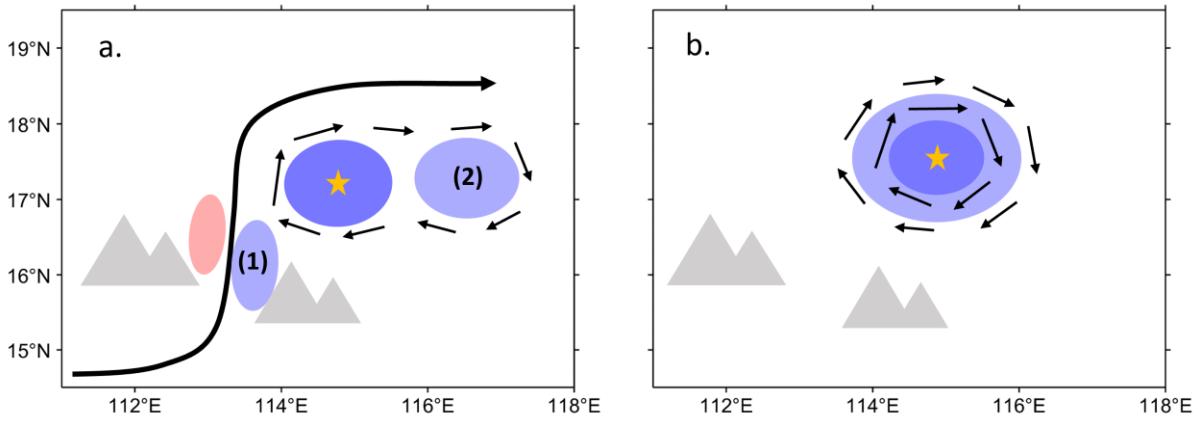

FIG. 15. Schematic diagram of eddy re-intensification. (a) Eddy-current and eddy-eddy interactions during intensification process. (b) After intensification. The shading color denotes the relative vorticity, with warm and cool color tones representing positive and negative values, respectively. The numbers in (a) represent the different sources of negative vorticity. The yellow star marks the center of the Kuroshio anticyclonic eddy. Black arrows indicate the current flow. The gray triangles indicate the Xisha and Zhongsha islands.

Acknowledgments

This work is supported by the National Natural Science Foundation of China (42430401, 42276026, 42476004), the Southern Marine Science and Engineering Guangdong Laboratory (Guangzhou) (2019BT02H594), the Chinese Academy of Sciences (XDA0370101, XBD42010304, SCSIO202201, SCSIO202204, SCSIO2023HC07), Guangdong Natural Science Funds for Distinguished Young Scholar (2024B1515020037), and Guangdong Basic and Applied Basic Research Foundation (2023A1515012691, 2024A1515010453). Cruise data were collected onboard R/V Shiyan-1, R/V Shiyan-3, and R/V Shiyan-6 implementing the Open Research Cruise NORC2021-302 supported by NSFC Ship-time Sharing Projects (42049907).

Data Availability Statement

The cruise observation data used in this study were obtained from https://data.scsio.ac.cn/metaData-detail/1790664041362321408. The satellite SLA and surface geostrophic velocity data were available at https://doi.org/10.48670/moi-00148. The Argo profile data were downloaded from https://fleetmonitoring.euro-argo.eu/float/2902711. The *WOA18* data can be found at https://www.ncei.noaa.gov/products/world-ocean-atlas. The CMEMS reanalysis data were available at https://data.marine.copernicus.eu/products. We

appreciate the provision of these publicly available datasets.

References

Bosse, A., I. Fer, J. M. Lilly, and H. Søiland, 2019: Dynamical controls on the longevity of a non-linear vortex: The case of the Lofoten Basin Eddy. *Sci. Rep.*, **9**, 13448, https://doi.org/10.1038/s41598-019-49599-8

Caruso, M. J., G. G. Gawarkiewicz, and R. C. Beardsley, 2006: Interannual variability of the Kuroshio intrusion in the South China Sea. *J. Oceanogr.*, **62**, 559–575, https://doi.org/10.1007/s10872-006-0076-0

Centurioni, L. R., P. P. Niiler, and D. K. Lee, 2004: Observations of inflow of Philippine Sea surface water into the South China Sea through the Luzon Strait. *J. Phys. Oceanogr.*, **34**(1), 113–121, https://doi.org/10.1175/1520-0485(2004)034<0113>2.0.CO;2

Chelton, D. B., M. G. Schlax, R. M. Samelson, and R. A. de Szoeke, 2007: Global observations of large oceanic eddies. *Geophys. Res. Lett.*, **34**(15), https://doi.org/10.1029/2007GL030812

——, M. G. Schlax, and R. M. Samelson, 2011: Global observations of nonlinear mesoscale eddies. *Prog. Oceanogr.*, **91**(2), 167–216, https://doi.org/10.1016/j.pocean.2011.01.002

Chen, G., Y. Hou, and X. Chu, 2011: Mesoscale eddies in the South China Sea: Mean properties, spatiotemporal variability, and impact on thermohaline structure. *J. Geophys. Res. Oceans*, **116**(C6), https://doi.org/10.1029/2010JC006716

——, ——, ——, P. Qi, and P. Hu, 2009: The variability of eddy kinetic energy in the South China Sea deduced from satellite altimeter data. *Chinese J. Oceanol. Limnol.*, **27**(4), 943–954, https://doi.org/10.1007/s00343-009-9297-6

Cheng, X., and Y. Qi, 2010: Variations of eddy kinetic energy in the South China Sea. *J. Oceanogr.*, **66**, 85–94, https://doi.org/10.1007/s10872-010-0007-y

Chu, P. C., and C. Fan, 2001: Low salinity, cool-core cyclonic eddy detected northwest of Luzon during the South China Sea Monsoon Experiment (SCSMEX) in July 1998. *J. Oceanogr.*, **57**, 549–563, https://doi.org/10.1023/A:1021251519067

Chu, X., H. Xue, Y. Qi, G. Chen, Q. Mao, D. Wang, and F. Chai, 2014: An exceptional anticyclonic eddy in the South China Sea in 2010. *J. Geophys. Res. Oceans*, **119**, 881–897, https://doi.org/10.1002/2013JC009314

——, G. Chen, and Y. Qi, 2020: Periodic mesoscale eddies in the South China Sea. *J. Geophys. Res. Oceans*, **125**, e2019JC015139, https://doi.org/10.1029/2019JC015139

Dong, C., J. C. McWilliams, Y. Liu, and D. Chen, 2014: Global heat and salt transports by eddy movement. *Nat. Commun.*, **5**(1), 3294, https://doi.org/10.1038/ncomms4294

Fu, M., C. Dong, J. Dong, and W. Sun, 2023: Analysis of mesoscale eddy merging in the subtropical northwest Pacific using satellite remote sensing data. *Remote Sens.,* **15**(17), 4307, https://doi.org/10.3390/rs15174307.

Gaube, P., D. B. Chelton, P. G. Strutton, and M. J. Behrenfeld, 2013: Satellite observations of chlorophyll, phytoplankton biomass, and Ekman pumping in nonlinear mesoscale eddies. *J. Geophys. Res. Oceans*, **118**(12), 6349–6370, https://doi.org/10.1002/2013JC009027

He, Q., H. Zhan, S. Cai, and G. Zha, 2016: On the asymmetry of eddy-induced surface chlorophyll anomalies in the southeastern Pacific: The role of eddy-Ekman pumping. *Prog. Oceanogr.*, **141**, 202–211, https://doi.org/10.1016/j.pocean.2015.12.012

Hu, J., J. Gan, Z. Sun, J. Zhu, and M. Dai, 2011: Observed three-dimensional structure of a cold eddy in the southwestern South China Sea. *J. Geophys. Res. Oceans*, **116**(C5), https://doi.org/10.1029/2010JC006810

Jia, Y., and Q. Liu, 2004: Eddy shedding from the Kuroshio bend at Luzon Strait. *J. Oceanogr.*, **60**, 1063–1069, https://doi.org/10.1007/s10872-005-0014-6

——, ——, and W. Liu, 2005: Primary study of the mechanism of eddy shedding from the Kuroshio bend in Luzon Strait. *J. Oceanogr.*, **61**, 1017–1027, https://doi.org/10.1007/s10872-006-0018-x

——, and E. P. Chassignet, 2011: Seasonal variation of eddy shedding from the Kuroshio intrusion in the Luzon Strait. *J. Oceanogr.*, **67**, 601–611, https://doi.org/10.1007/s10872-011-0060-1

Lellouche, J. M., E. Greiner, R. Bourdallé-Badie, G. Garric, A. Melet, M. Drévillon, ... and P. Y. L. T., 2021: The Copernicus global 1/12° oceanic and sea ice GLORYS12 reanalysis. *Front. Earth Sci.*, **9**, 698876, https://doi.org/10.3389/feart.2021.698876

Leyba, I. M., M. Saraceno, and S. A. Solman, 2017: Air-sea heat fluxes associated to mesoscale eddies in the Southwestern Atlantic Ocean and their dependence on different regional conditions. *Clim. Dyn.*, **49**, 2491–2501, https://doi.org/10.1007/s00382-016-3460-5

Li, L., W. D. Nowlin Jr., and S. Jilan, 1998: Anticyclonic rings from the Kuroshio in the South China Sea. *Deep Sea Res. I: Oceanogr. Res. Papers*, **45**(9), 1469–1482, https://doi.org/10.1016/S0967-0637(98)00026-0

——, and B. Y. Wu, 1989: A Kuroshio loop in South China Sea?—On circulations of the north-eastern South China Sea (in Chinese with English abstract). *J. Oceanogr. Taiwan Strait*,

8(1), 89–95.

Lin, X., C. Dong, D. Chen, Y. Liu, J. Yang, B. Zou, and Y. Guan, 2015: Three-dimensional properties of mesoscale eddies in the South China Sea based on eddy-resolving model output. *Deep Sea Res. I: Oceanogr. Res. Papers*, **99**, 46–64, https://doi.org/10.1016/j.dsr.2015.01.007

McGillicuddy Jr, D. J., 2016: Mechanisms of physical-biological-biogeochemical interaction at the oceanic mesoscale. *Annu. Rev. Mar. Sci.*, **8**, 125–159, https://doi.org/10.1146/annurev-marine-010814-015606

Nan, F., H. Xue, F. Chai, L. Shi, M. Shi, and P. Guo, 2011a: Identification of different types of Kuroshio intrusion into the South China Sea. *Ocean Dyn.*, **61**(9), 1291–1304, https://doi.org/10.1007/s10236-011-0426-3

——, ——, ——, D. Wang, F. Yu, M. Shi, ... and P. Xiu, 2013: Weakening of the Kuroshio intrusion into the South China Sea over the past two decades. *J. Climate*, **26**(20), 8097–8110, https://doi.org/10.1175/JCLI-D-12-00315.1

——, ——, P. Xiu, F. Chai, M. Shi, and P. Guo, 2011b: Oceanic eddy formation and propagation southwest of Taiwan. *J. Geophys. Res. Oceans*, **116**(C12), https://doi.org/10.1029/2011JC007386

——, ——, and F. Yu, 2015: Kuroshio intrusion into the South China Sea: A review. *Prog. Oceanogr.*, **137**, 314–333, https://doi.org/10.1016/j.pocean.2014.05.012

Nencioli, F., Kuwahara, V. S., Dickey, T. D., Rii, Y. M., and Bidigare, R. R, 2008: Physical dynamics and biological implications of a mesoscale eddy in the lee of Hawai'i: Cyclone Opal observations during E-Flux III. *Deep-Sea Res. II*, **55**(10-13), 1252-1274, https://doi.org/10.1016/j.dsr2.2008.02.003

Ni, Q., X. Zhai, X. Jiang, and D. Chen, 2021: Abundant cold anticyclonic eddies and warm cyclonic eddies in the global ocean. *J. Phys. Oceanogr.*, **51**(9), 2793–2806, https://doi.org/10.1175/JPO-D-21-0010.1

Potter, H., C. Y. Hsu, and S. F. DiMarco, 2021: Rapid dissipation of a Loop Current eddy due to interaction with a severe Gulf of Mexico hurricane. *Ocean Dyn.*, **71**(9), 911–922, https://doi.org/10.1007/s10236-021-01471-y

Qi, Y., H. Mao, Y. Du, X. Li, Z. Yang, K. Xu, ... and H. Xing, 2022: A lens-shaped, cold-core anticyclonic surface eddy in the northern South China Sea. *Front. Mar. Sci.*, **9**, 976273, https://doi.org/10.3389/fmars.2022.976273

Qiao, J., C. Qiu, D. Wang, Y. Huang, and X. Zhang, 2023: Multi-stage development within

anisotropy insight of an anticyclone eddy in the northwestern South China Sea in 2021. Geophys. *Res. Lett.*, **50**(19), e2023GL104736, https://doi.org/10.1029/2023GL104736

Qiu, C., H. Mao, H. Liu, Q. Xie, J. Yu, D. Su, ... and S. Lian, 2019: Deformation of a warm eddy in the northern South China Sea. *J. Geophys. Res. Oceans*, **124**(8), 5551–5564, https://doi.org/10.1029/2019JC015288

Qu, T., Y. Y. Kim, M. Yaremchuk, T. Tozuka, A. Ishida, and T. Yamagata, 2004: Can Luzon Strait transport play a role in conveying the impact of ENSO to the South China Sea? *J. Climate*, **17**(18), 3644–3657, https://doi.org/10.1175/1520-0442(2004)017<3644>2.0.CO;2

——, H. Mitsudera, and T. Yamagata, 2000: Intrusion of the North Pacific waters into the South China Sea. *J. Geophys. Res.*, **105**(C3), 6415–6424, https://doi.org/10.1029/1999jc900323

Robinson, A. R., 1983: Overview and summary of eddy science. In *Eddies in marine science* (pp. 3–15). Springer Berlin Heidelberg.

Sheng, C., J. Jiao, X. Luo, J. Zuo, L. Jia, and J. Cao, 2023: Offshore freshened groundwater in the Pearl River estuary and shelf as a significant water resource. *Nat. Commun.*, **14**(1), 3781, https://doi.org/10.1038/s41467-023-39507-0

Sun, F., X. Xia, M. Simon, Y. Wang, H. Zhao, C. Sun, ... and M. Wu, 2022: Anticyclonic eddy driving significant changes in prokaryotic and eukaryotic communities in the South China Sea. *Front. Mar. Sci.*, **9**, 773548, https://doi.org/10.3389/fmars.2022.773548

Sun, M., F. Tian, Y. Liu, and G. Chen, 2017: An improved automatic algorithm for global eddy tracking using satellite altimeter data. *Remote Sens.*, **9**(3), 206, https://doi.org/10.3390/rs9030206

Sun, Z., J. Hu, Z. Chen, J. Zhu, L. Yang, X. Chen, and X. Wu, 2021: A strong Kuroshio intrusion into the South China Sea and its accompanying cold-core anticyclonic eddy in winter 2020–2021. *Remote Sens.*, **13**(14), 2645, https://doi.org/10.3390/rs13142645

Sun, Z., Zhang, Z., Qiu, B., Zhang, X., Zhou, C., Huang, X., ... and Tian, J., 2020: Three-dimensional structure and interannual variability of the Kuroshio Loop Current in the northeastern South China Sea. *J. Phys. Oceanogr.*, **50**(9), 2437–2455, https://doi.org/10.1175/JPO-D-20-0058.1

Tang, T., Zhang, Z., Zhang, J., Zhang, X., Sun, Z., & Feng, Z., 2024: Submesoscale processes in the Kuroshio Loop Current: Roles in energy cascade and salt and heat transports. *J. Geophys. Res. Oceans*, **129**(7), e2023JC020226, https://doi.org/10.1029/2023JC020226

Trodahl, M., P. E. Isachsen, J. M. Lilly, J. Nilsson, and N. M. Kristensen, 2020: The

regeneration of the Lofoten Vortex through vertical alignment. *J. Phys. Oceanogr.*, **50**(9), 2689–2711, https://doi.org/10.1175/JPO-D-20-0029.1

Wang, D., H. Xu, J. Lin, and J. Hu, 2008: Anticyclonic eddies in the northeastern South China Sea during winter 2003/2004. *J. Oceanogr.*, **64**, 925–935, https://doi.org/10.1007/s10872-008-0076-3

Wang, G., J. Su, and P. C. Chu, 2003: Mesoscale eddies in the South China Sea observed with altimeter data. *Geophys. Res. Lett.*, **30**(21), https://doi.org/10.1029/2003GL018532

Wang, X., Y. Du, Y. Zhang, A. Wang, and T. Wang, 2021: Influence of two Eddy Pairs on high-salinity water intrusion in the northern South China Sea during fall-winter 2015/2016. *J. Geophys. Res. Oceans*, **126**(6), e2020JC016733, https://doi.org/10.1029/2020JC016733

——, ——, ——, T. Wang, M. Wang, and Z. Jing, 2023: Subsurface anticyclonic eddy transited from Kuroshio shedding eddy in the northern South China Sea. *J. Phys. Oceanogr.*, **53**(3), 841–861, https://doi.org/10.1175/JPO-D-22-0106.1

Wang, Z. F., L. Sun, Q. Y. Li, and H. Cheng, 2019: Two typical merging events of oceanic mesoscale anticyclonic eddies. *Ocean Sci.*, **15**(6), 1545–1559, https://doi.org/10.5194/os-15-1545-2019

Wu, C. R., 2013: Interannual modulation of the Pacific Decadal Oscillation (PDO) on the low-latitude western North Pacific. *Prog. Oceanogr.*, **110**, 49–58, https://doi.org/10.1016/j.pocean.2012.12.001

Xiu, P., and F. Chai, 2011: Modeled biogeochemical responses to mesoscale eddies in the South China Sea. *J. Geophys. Res. Oceans*, **116**(C10), https://doi.org/10.1029/2010JC006800

——, ——, L. Shi, H. Xue, and Y. Chao, 2010: A census of eddy activities in the South China Sea during 1993–2007. *J. Geophys. Res. Oceans*, **115**(C3), https://doi.org/10.1029/2009JC005657

Xue, H., F. Chai, N. Pettigrew, D. Xu, M. Shi, and J. Xu, 2004: Kuroshio intrusion and the circulation in the South China Sea. *J. Geophys. Res.*, **109**(C2), https://doi.org/10.1029/2002jc001724

Yang, Q., M. Nikurashin, H. Sasaki, H. Sun, and J. Tian, 2019: Dissipation of mesoscale eddies and its contribution to mixing in the northern South China Sea. *Sci. Rep.*, **9**(1), 556, https://doi.org/10.1038/s41598-018-36610-x

Yang, Y., L. Zeng, and Q. Wang, 2021: How much heat and salt are transported into the South China Sea by mesoscale eddies? *Earth's Future*, **9**(7), e2020EF001857, https://doi.org/10.1029/2020EF001857

Yuan, D., W. Han, and D. Hu, 2006: Surface Kuroshio path in the Luzon Strait area derived from satellite remote sensing data. *J. Geophys. Res. Oceans*, **111**(C11), https://doi.org/10.1029/2005JC003412

——, ——, and ——, 2007: Anti-cyclonic eddies northwest of Luzon in summer–fall observed by satellite altimeters. *Geophys. Res. Lett.*, **34**(13), https://doi.org/10.1029/2007GL029401

Zhang, Z., W. Wang, and B. Qiu, 2014: Oceanic mass transport by mesoscale eddies. *Science*, **345**(6194), 322–324, https://doi.org/10.1126/science.1252418

Zhang, Z., J. Tian, B. Qiu, W. Zhao, P. Chang, D. Wu, and X. Wan, 2016: Observed 3D structure, generation, and dissipation of oceanic mesoscale eddies in the South China Sea. *Sci. Rep.*, **6**(1), 24349, https://doi.org/10.1038/srep24349

——, W. Zhao, B. Qiu, and J. Tian, 2017: Anticyclonic eddy sheddings from Kuroshio loop and the accompanying cyclonic eddy in the northeastern South China Sea. *J. Phys. Oceanogr.*, **47**(6), 1243–1259, https://doi.org/10.1175/jpo-d-16-0185.1

——, ——, J. Tian, and X. Liang, 2013: A mesoscale eddy pair southwest of Taiwan and its influence on deep circulation. *J. Geophys. Res. Oceans*, **118**(12), 6479–6494, https://doi.org/10.1002/2013JC008994